

Dear Editor,

Thanks for pointing out remaining inconsistencies in the paper. Below is our detailed reply (in blue) to the points raised (in black):

l. 162, 168, 186, 189 and elsewhere: Please replace 1/2", 1/4", 1/8", 1/16" with 1/2 inch, 1/4 inch, etc. for clarity.

→ done

l. 163, 213, 219 and elsewhere: Reference gas and pressure for the volumetric flow rate should be given (273 K, 1 bar?).

→ The requested information has been added. Indeed the flow rates are reported under standard conditions (273 K, 1 bar).

l. 171: Hasn't this been published?

Brand WA, Rothe M, Sperlich P, Strube M, Wendeborg M (2016) Automated simultaneous measurement of the  $\delta^{13}\text{C}$  and  $\delta^2\text{H}$  values of methane and the  $\delta^{13}\text{C}$  and  $\delta^{18}\text{O}$  values of carbon dioxide in flask air samples using a new multi cryo-trap/gas chromatography/isotope ratio mass spectrometry system Rapid Commun Mass Spectrom 30:1523 10.1002/rcm.7587

→ The reference has been updated in the final manuscript.

l. 231 + 237: This use of the  $\pm$  symbol (and the view of referee #1) is incorrect. Repeatability (and uncertainty) is always a positive, so the  $\pm$  sign should be deleted. See also the Guide to the Expression of Uncertainty in Measurement (GUM),

<http://www.bipm.org/en/publications/guides/gum.html>.

→ done

l. 250 + 251: What are the uncertainties of these values?

→ The respective uncertainty values have been added.

l. 277: What is the uncertainty associated with the value of 1.58 ‰?

→ The respective uncertainty values have been added.

l. 284 + 287: What was the matrix gas of these calibration gases? 80 % N<sub>2</sub> + 20 % O<sub>2</sub>? And what gas was used for dilution?

→ The gas matrix of the calibration gases was synthetic air: 79.5% N<sub>2</sub> / 20.5% O<sub>2</sub>. Synthetic air was also used for dilution. This information has been added.

l. 300: What was the matrix gas of these target gases?

→ The target gases are pressurized air samples. This information has been added.

l. 310: Please correct spelling of Eulerian.

→ done

l. 311, 322 and 332: Please clarify what tracers are the model - CH<sub>4</sub>, <sup>13</sup>CH<sub>4</sub> & CDH<sub>3</sub>; CH<sub>4</sub>,  $\delta^{13}\text{C}$  &  $\delta(\text{D})$ ; <sup>12</sup>CH<sub>4</sub>, <sup>13</sup>CH<sub>4</sub> and <sup>12</sup>CDH<sub>3</sub>? Strictly speaking only the latter combination be correct, but if the model is linear, the error made due to replacing <sup>12</sup>CH<sub>4</sub> with CH<sub>4</sub> is small (about 1 % of the variations in the  $\delta^{13}\text{C}$  value, so probably less than 0.01 %).

→ line 335 (new manuscript) states explicitly which tracers are used in the TM5 model. FLEXPART-COSMO does not model isotopic composition, but only CH<sub>4</sub>. The isotope information is later "added" as described in lines 395-397. The misleading statement "δD was only simulated with FLEXPART-COSMO" was therefore removed.

l. 356: Electronic state symbols such as 1D in O(1D) should be written in roman (upright) font. <http://iupac.org/cms/wp-content/uploads/2016/01/ICTNS-On-the-use-of-italic-and-roman-fonts-for-symbols-in-scientific-text.pdf>

→ corrected

l. 444: This was changed back to the original pre-ACPD manuscript. As I pointed out then, "intercomparison" is a pleonasm and does not have any metrological meaning. It should be replaced with "Comparison" or "Intercalibration". The latter term would imply that one dataset is designated as a more reliable "reference" dataset. If no such assignment is made, then the term "comparison" should be chosen.

→ corrected

l. 511: Space missing before "well". Please add a root-mean-squared deviation (RMSD) and/or  $R^2$  value or similar figure of merit to quantify "well" better.

→ The typo has been corrected.

We agree that this is a qualitative statement, but since this is indeed a qualitative and general description of the agreement (simply looking at the figure) we think that it is adequate here. Adding simply a number (RMSD or  $R^2$  value) will not add much value, unless we also provide a background what value would mean good agreement for such a comparison. However, as we do not analyze the model-data agreement in the mole fraction in more detail, but concentrate on the isotope signals, we think that the general statement that the model captures the variability well is sufficient here and a metric for the agreement is not needed.

Before the acknowledgements, please add a section on data availability, as per the ACP Data Policy ([http://www.atmospheric-chemistry-and-physics.net/about/data\\_policy.html#data\\_availability](http://www.atmospheric-chemistry-and-physics.net/about/data_policy.html#data_availability)). The supplementary information seems to contain the data from only one of the two instruments used. The data from the other instrument should be added as separate files.

→ The data availability section has been added: The data used for the scientific analysis of this paper are available as supplementary information to this paper and at <https://www.projects.science.uu.nl/atmosphereclimate/Data.php>

We note that the data that we provided actually contain the merged data of both instruments, as they are used as one single dataset for scientific analysis.

1 **In-situ observations of the isotopic composition of methane at the**  
2 **Cabauw tall tower site**

3

4 Thomas Röckmann<sup>1,\*</sup>, Simon Eyer<sup>2,\*</sup>, Carina van der Veen<sup>1</sup>, Maria E. Popa<sup>1</sup>, Béla  
5 Tuzson<sup>2</sup>, Guillaume Monteil<sup>1,3</sup>, Sander Houweling<sup>1</sup>, Eliza Harris<sup>2</sup>, Dominik  
6 Brunner<sup>2</sup>, Hubertus Fischer<sup>7</sup>, Giulia Zazzeri<sup>4</sup>, David Lowry<sup>4</sup>, Euan G. Nisbet<sup>4</sup>, Willi  
7 A. Brand<sup>5</sup>, Jaroslav M. Necki<sup>6</sup>, Lukas Emmenegger<sup>2</sup> and Joachim Mohn<sup>2</sup>

8

9 <sup>1</sup> Utrecht University (UU), Institute for Marine and Atmospheric Research  
10 Utrecht (IMAU), The Netherlands

11 <sup>2</sup> Empa, Laboratory for Air Pollution / Environmental Technology, Dübendorf,  
12 Switzerland

13 <sup>3</sup> now at Department of Physical Geography and Ecosystem Science, Lund  
14 University, Lund, Sweden

15 <sup>4</sup> Royal Holloway University of London (RHUL), Department of Earth Sciences,  
16 Egham, UK

17 <sup>5</sup> Max-Planck-Institute (MPI) for Biogeochemistry, Jena, Germany

18 <sup>6</sup> Environmental Physics Group, Faculty of Physics and Applied Computer  
19 Science, AGH University of Science and Technology, Krakow, Poland

20 <sup>7</sup> University of Bern, Climate and Environmental Physics, Bern, Switzerland

21

22 \*These authors contributed equally to this work

23

24

25 **Abstract**

26 High precision analyses of the isotopic composition of methane in ambient air  
27 can potentially be used to discriminate between different source categories. Due  
28 to the complexity of isotope ratio measurements, such analyses have generally  
29 been performed in the laboratory on air samples collected in the field. This poses  
30 a limitation on the temporal resolution at which the isotopic composition can be  
31 monitored with reasonable logistical effort. Here we present the performance of  
32 a dual isotope ratio mass spectrometric system (IRMS) and a quantum cascade  
33 laser absorption spectroscopy (QCLAS) based technique for in-situ analysis of  
34 the isotopic composition of methane under field conditions. Both systems were  
35 deployed at the Cabauw experimental site for atmospheric research (CESAR) in  
36 the Netherlands and performed in-situ, high-frequency (approx. hourly)  
37 measurements for a period of more than 5 months. The IRMS and QCLAS  
38 instruments were in excellent agreement with a slight systematic offset of (+0.25  
39  $\pm$  0.04) ‰ for  $\delta^{13}\text{C}$  and (-4.3  $\pm$  0.4) ‰ for  $\delta\text{D}$ . This was corrected for, yielding a  
40 combined dataset with more than 2500 measurements of both  $\delta^{13}\text{C}$  and  $\delta\text{D}$ . The  
41 high precision and temporal resolution dataset does not only reveal the  
42 overwhelming contribution of isotopically depleted agricultural  $\text{CH}_4$  emissions  
43 from ruminants at the Cabauw site, but also allows the identification of specific  
44 events with elevated contributions from more enriched sources such as natural  
45 gas and landfills. The final dataset was compared to model calculations using the  
46 global model TM5 and the mesoscale model FLEXPART-COSMO. The results of  
47 both models agree better with the measurements when the TNO-MACC emission  
48 inventory is used in the models than when the EDGAR inventory is used. This  
49 suggests that high-resolution isotope measurements have the potential to  
50 further constrain the methane budget, when they are performed at multiple sites  
51 that are representative for the entire European domain.

## 52 **1. Introduction**

53 The global increase of the important greenhouse gas methane in the atmosphere  
54 since the beginning of the industrial period is very well established  
55 (Dlugokencky et al., 2009; Dlugokencky et al., 1996; Dlugokencky et al., 1998;  
56 Etheridge et al., 1998; Khalil et al., 2007; Louergue et al., 2008; MacFarling  
57 Meure et al., 2006; Rasmussen and Khalil, 1981; Spahni et al., 2005). The existing  
58 CH<sub>4</sub> mole fraction measurement data enable accurate assessment of the source-  
59 sink imbalance through time, and together with the estimated total sink strength,  
60 they allow for a top-down constraint on the global source of methane to the  
61 atmosphere (Bergamaschi et al., 2013; Houweling et al., 2014). Bottom-up  
62 estimates of the global methane budget carry much larger uncertainties, which  
63 are inherent to the assumptions made in the extrapolation of local scale  
64 measurements to larger scales (Bruhwiler et al., 2014; Kirschke et al., 2013;  
65 Nisbet et al., 2014). The advantage of bottom-up estimates is, however, the  
66 possibility to distinguish different sources and to link observations to process-  
67 level understanding of the emissions.

68 An independent approach for distinguishing between source categories of CH<sub>4</sub> is  
69 the analysis of its isotopic composition, which is strongly linked to the  
70 source/sink processes. This is particularly true for methane from biogenic,  
71 thermogenic and pyrogenic sources (Gros et al., 2004; Houweling et al., 2008;  
72 Quay et al., 1999; Sapart et al., 2012). A more detailed differentiation within one  
73 source category, e.g. biogenic CH<sub>4</sub>, for emissions from wetlands, ruminants, rice  
74 paddies or termites, however, is complicated because of the overlap of the  
75 respective isotopic source signatures. Further complications arise because  
76 individual source signatures can show pronounced dependence on  
77 environmental parameters and metabolized substrates (Kawagucci et al., 2014;  
78 Klevenhusen et al., 2010). In addition to the source contributions, the sink  
79 processes (mainly chemical removal by the hydroxyl radical (OH), but also soil  
80 deposition and stratospheric loss) also affect the isotopic composition of  
81 atmospheric methane (Brenninkmeijer et al., 1995; Röckmann et al., 2011;  
82 Saueressig et al., 1996; Saueressig et al., 2001; Snover and Quay, 2000).  
83 Nevertheless, over the past decades, numerous studies have shown the potential  
84 of isotope measurements to identify individual source categories from isotope

85 observations (Beck et al., 2012; Lassey et al., 1993; Tarasova et al., 2006;  
86 Umezawa et al., 2012b; Zazzeri et al., 2015) and to constrain budgets (Ferretti et  
87 al., 2005; Fischer et al., 2008; Houweling et al., 2008; Lassey et al., 2000; Lowe et  
88 al., 1994; Sapart et al., 2012; Umezawa et al., 2012a).

89 The isotopic composition is commonly reported in  $\delta$  notation, where  $\delta$  quantifies  
90 the relative deviation of an isotope ratio ( $^{13}R = ^{13}\text{C}/^{12}\text{C}$  for carbon isotopes and  $^2R$   
91  $= ^2\text{H}/^1\text{H}$ , abbreviated as D/H, for hydrogen isotopes) in a sample from a standard  
92 ratio. The international standard for reporting  $\delta(^{13}\text{C}, \text{CH}_4)$  values is Vienna Pee  
93 Dee Belemnite (VPDB,  $^{13}R_{\text{VPDB}} = 0.0112372$  (Craig, 1957)) and for  $\delta(\text{D}, \text{CH}_4)$  it is  
94 Vienna Standard Mean Ocean Water (VSMOW,  $^2R_{\text{VSMOW}} = 0.0020052$  (Baertschi,  
95 1976)).  $\delta(^{13}\text{C}, \text{CH}_4)$  and  $\delta(\text{D}, \text{CH}_4)$  are abbreviated as  $\delta^{13}\text{C}$  and  $\delta\text{D}$  in the following,  
96 and given in per mill (‰).  $\text{CH}_4$  mole fractions  $\chi(\text{CH}_4)$  are reported in  $\text{nmol/mol} =$   
97  $10^{-9}$  and  $\mu\text{mol/mol} = 10^{-6}$ . For interpretation of global or continental scale  
98 atmospheric data the expert group of the WMO/IAEA has set a scientifically  
99 desirable level of compatibility of 2  $\text{nmol/mol}$ , 0.02 ‰ and 1 ‰ for  $\text{CH}_4$   
100 fraction,  $\delta^{13}\text{C}$  and  $\delta\text{D}$ , respectively (WMO, 2014). For regionally focused studies  
101 with large local fluxes, extended compatibility goals of 5  $\text{nmol/mol}$ , 0.2 ‰ and 5  
102 ‰ for  $\chi(\text{CH}_4)$ ,  $\delta^{13}\text{C}$  and  $\delta\text{D}$  were defined.

103 Due to the complexity of the involved measurement techniques,  $\text{CH}_4$  isotope  
104 measurements have been limited mostly to relatively low frequency sampling in  
105 the field followed by isotope analysis in the laboratory (Bock et al., 2010; Brass  
106 and Röckmann, 2010; Sapart et al., 2011; Sperlich et al., 2013; Umezawa et al.,  
107 2009; Yamada et al., 2003). For many decades, the dominant method for high  
108 precision isotope analysis of atmospheric methane was isotope ratio mass  
109 spectrometry. In particular, the development of continuous-flow IRMS in the past  
110 two decades (Merritt et al., 1994; Merritt et al., 1995) has greatly increased the  
111 throughput of IRMS methods, making this the technique of choice in most  
112 laboratories, also because of the small sample amounts required.

113 Recently, mid-infrared laser absorption spectroscopy has proven its potential for  
114 high precision isotope ratio analysis. First attempts of measuring the isotopic  
115 composition of methane (Bergamaschi et al., 1998a; 1998b; 1994) were  
116 restricted to enhanced  $\text{CH}_4$  fractions ( $>50 \mu\text{mol/mol}$  for  $\delta^{13}\text{C}$  and  $>2000$

117  $\mu\text{mol/mol}$  for  $\delta\text{D}$ ) and required cryogenic cooling for both the laser source and  
118 the detector, which impeded in-situ and long-term applications. The invention of  
119 room temperature, quantum cascade laser (QCL) sources has triggered the  
120 development of a novel generation of spectrometers suitable for in-situ analysis  
121 of the isotopic composition of greenhouse gases (Eyer and al, 2015; Tuzson et al.,  
122 2008; Wächter et al., 2008). Their capability of high-temporal resolution led to  
123 new applications aiming for source attribution (Mohn et al., 2012; Tuzson et al.,  
124 2011; Wolf et al., 2015). The advantages of in-situ measurements are particularly  
125 apparent in combination with atmospheric modeling techniques, which enables  
126 the identification of specific source regions (Rigby et al., 2012; Sturm et al.,  
127 2013). Similarly, high-frequency, high-precision  $\text{CH}_4$  isotope data are expected to  
128 greatly reduce uncertainties of national and global source estimations, as  
129 demonstrated in an observing system simulation experiment (Rigby et al., 2012).

130 In this paper we present the analytical setup and results of a 5-month campaign  
131 at the Cabauw tall tower site in the Netherlands, where the isotopic composition  
132 ( $\delta^{13}\text{C}$  and  $\delta\text{D}$ ) of  $\text{CH}_4$  was measured with two instruments, one IRMS system  
133 developed at Utrecht University and one QCLAS-instrument developed at Empa.  
134 The compatibility of the two analytical techniques for  $\text{CH}_4$  mole fractions,  $\delta^{13}\text{C}$ -  
135  $\text{CH}_4$  and  $\delta\text{D}$ - $\text{CH}_4$  is assessed and the obtained high-resolution isotope dataset is  
136 exploited using a novel moving Keeling plot method. A comparison of  
137 measurement results with calculations from two different models (TM5 and  
138 FLEXPART-COSMO) and two emission inventories (EDGAR, TNO-MACC)  
139 indicates the potential of this approach to better constrain on isotope source  
140 signatures and emissions in atmospheric models.

## 141 **2. Methods**

### 142 **2.1. Site description**

143 The 213 m tall tower is the central construction of the Cabauw Experimental Site  
144 for Atmospheric Research (CESAR, <http://www.cesar-observatory.nl/>,  $51^\circ 58' \text{N}$ ,  
145  $4^\circ 55' \text{E}$ , 2 m a.s.l.). The CESAR site is dedicated to atmospheric research and  
146 hosts a wide variety of instruments for in situ and remote sensing measurements  
147 of meteorological parameters, trace gases, pollutants, aerosols, and clouds. The

148 site is located in an agricultural landscape, with CH<sub>4</sub> emissions originating from  
149 ruminants and other agricultural activities, but also from the peaty soil and the  
150 drainage ditches between the surrounding fields (Peltola et al., 2014). The small  
151 town Lopik (~7500 inhabitants) is located 1 km east of the tower. Population  
152 and road density increase steeply further away from the tower towards the  
153 country's major cities: Utrecht (at about 20 km distance), Rotterdam (30 km), the  
154 Hague (40 km) and Amsterdam (45 km). An estimated seven million people  
155 inhabit these cities and their many neighboring settlements. The location and  
156 surroundings are described in more detail in (Peltola et al., 2014; Peltola et al.,  
157 2015; Vermeulen et al., 2011). The instruments were operated in a room on the  
158 ground floor of the CESAR building. Since this room is not commonly used as  
159 laboratory, it has air-conditioning with limited cooling capacity and the  
160 temperature varied between 25 °C and 30 °C.

## 161 2.2. Air sampling at the Cabauw tall tower

162 Air was continuously drawn through ½ [inch](#) o.d. (outer diameter) Dekabon  
163 tubing from 20 m height at a total flow of 16 l min<sup>-1</sup> (STP) provided by a Varian  
164 scroll pump (Agilent Technologies Inc., USA). The sample gas flow was adjusted  
165 by means of a flow restriction at the inlet of the pump in order to maintain the  
166 pressure in the sampling line above 950 hPa. The sample gas flows for the  
167 methane isotope analyzers were branched off upstream of the scroll pump and  
168 the restriction, using ¼ [inch](#) o.d. Dekabon lines.

## 169 2.3. IRMS system

170 The new IRMS method for δ<sup>13</sup>C and δD analysis of atmospheric CH<sub>4</sub> is based on  
171 the ISAAC system as developed at the MPI for Biogeochemistry in Jena (Brand et  
172 al., 2016). Importantly, the system does not require liquid nitrogen coolant for  
173 the preconcentration and focusing steps, but uses a massive copper block cooled  
174 down to about -145 °C, to which the cold traps for preconcentration and cryo-  
175 focussing are connected via standoffs (see 2.3.1). This cold assembly is contained  
176 in an evacuated steel Dewar to prevent condensation of moisture. During the  
177 campaign, the extraction unit and two IRMS instruments (Thermo Delta Plus XL  
178 for hydrogen isotopes and Thermo Delta Plus XP for carbon isotopes, both

roeckman 1/8/2016 14:02

Deleted: "

roeckman 1/8/2016 14:02

Deleted: "



181 Thermo Fisher Scientific Inc., Germany) were operated at the CESAR site. The  
182 system is schematically shown in Fig. 1.

### 183 2.3.1. Cryogenic trapping

184 A Polycold compact cooler compressor (Brooks Automation Inc., USA), filled with  
185 coolant PT-30, cooled a cold end on which a copper cylinder (70 mm diameter,  
186 85 mm height, 3 kg) was mounted. In this configuration, the copper block  
187 reached a temperature of -145 °C. The pre-concentration trap (PreCon) was a 10  
188 cm 1/8, inch SS tube filled with 4 cm 60/80 mesh HayeSep D in the center and 3  
189 cm 60/80 glass beads on each end. It was connected with Valco fittings and the  
190 packing material was retained in the trap using removable frits (CEF1F, Valco  
191 Instruments Company Inc., USA). The focus trap (Focus) was a 10 cm 1/16, inch  
192 SS tube filled with 2 cm HayeSep D and 4 cm glass beads at both ends, connected  
193 with Valco fittings (ECEP211.0F, Valco Instruments Company Inc., USA). The  
194 traps could be heated with 0.5 m Thermsys heating wire wrapped around the  
195 tubes. The PreCon and Focus trapping units were glued together with a PT-100  
196 temperature sensor in heat - conducting two component epoxy on a brass  
197 standoff. These brass standoffs were mounted to the copper cylinder. In the  
198 "trapping" configuration the temperatures of the traps were usually kept at -135  
199 °C.

### 200 2.3.2. Measurement procedure

201 A 3-port 2-position Valco valve (3PV, Fig. 1) selected either ambient air drawn  
202 from the tower through a Mg(ClO<sub>4</sub>)<sub>2</sub> dryer, or cylinder air that was injected via  
203 one port of an 8-port multiposition Valco valve (MPV). To check the system  
204 performance, a reference air cylinder (Ref) was measured alternately with  
205 ambient air, and three other target gas cylinders were measured occasionally.  
206 The inlet line was connected to a 4-port 2-position Valco valve (4PV1), which  
207 directed either Helium (He, BIP quality, Air Products and Chemicals Inc., USA) or  
208 the selected airflow to the PreCon unit, which was connected in the loop position  
209 of a 6-port 2-position Valco valve (6PV). All He and air flows were controlled by  
210 MKS mass flow controllers (MFC, MKS Instruments Inc., USA).

211 The preconcentration and cryofocussing was done similarly to Brass and

roeckman 1/8/2016 14:02

Deleted: "

roeckman 1/8/2016 14:02

Deleted: "

214 Röckmann (2010). After flushing the inlet line with >20 ml air, the 6PV was  
215 switched to the load position and air was admitted to the PreCon unit. The  
216 duration of the air sampling for the IRMS system was 10 minutes at a flow rate of  
217 | 5 ml min<sup>-1</sup> for  $\delta^{13}\text{C}$  and 7 ml min<sup>-1</sup> for  $\delta\text{D}$  (273 K, 1 bar). The flow was provided  
218 by a Xavitech mini pump (P200-GAS-12V, Xavitech AB, Sweden). During this step,  
219 the temperature measured at the PreCon stayed below -132 °C. At this  
220 temperature CH<sub>4</sub> and several other trace species were retained on the HayeSep  
221 D, while the air matrix was efficiently flushed out.

222 After preconcentration, the PreCon unit was heated to -30 °C and a He flow of  
223 | 4 ml min<sup>-1</sup> (273 K, 1 bar) transported the CH<sub>4</sub> in 90 seconds to the Focus unit,  
224 which was held at a temperature <-137 °C. After transfer of the sample to the  
225 Focus, the 6PV was switched to the load position and the PreCon was heated to -  
226 10 °C to release any remaining trapped gases such as CO<sub>2</sub>.

227 The Focus was then heated to release the CH<sub>4</sub>, which was directed via 4PV2 and  
228 4VP3 either to the combustion oven and the Delta plus XP IRMS for <sup>13</sup>C analysis  
229 or to the pyrolysis oven and the Delta plus XL IRMS for D analysis.

230 For  $\delta\text{D}$  analysis, the CH<sub>4</sub> was injected into a pyrolysis tube furnace (1400 °C),  
231 where CH<sub>4</sub> was converted to H<sub>2</sub> and carbon. The H<sub>2</sub> entered the IRMS, after  
232 passing a 2 m CarboPLOT column at room temperature (RT) and a nafion dryer,  
233 via the GasBench interface. No krypton interference (Schmitt et al., 2013) could  
234 | be determined in this setup. The repeatability for  $\delta\text{D}$  was generally better than 2  
235 ‰ (reported as SD), based on consecutive analyses of reference air.

236 For  $\delta^{13}\text{C}$ , the CH<sub>4</sub> was injected from the cryofocus unit into a combustion oven  
237 containing a nickel / nickel oxide wire catalyst at 1100 °C, where the CH<sub>4</sub> was  
238 converted to CO<sub>2</sub> and H<sub>2</sub>O. The resulting gas mixture passed a nafion dryer and a  
239 10 m PoraPLOT Q column (5 °C) to eliminate interference from co-trapped  
240 krypton (Schmitt et al., 2013) before entering the IRMS via the GasBench  
241 | interface. The repeatability of  $\delta^{13}\text{C}$  was better than 0.07 ‰ (reported as SD),  
242 based on consecutive analyses of reference air.

243 The typical measurement order during the Cabauw campaign was Ref  $\delta^{13}\text{C}$  – Air  
244  $\delta^{13}\text{C}$  – Ref  $\delta\text{D}$  – Air  $\delta\text{D}$ . A full measurement cycle took 84 min. On a regular basis,  
245 pressurized air from a cylinder, applied as a target gas, was analyzed as a quality

roeckman 1/8/2016 14:20

Deleted: ±

roeckman 1/8/2016 14:20

Deleted: ±

248 control tool in order to monitor the long term stability of the analytical  
249 technique. The CH<sub>4</sub> mole fraction and isotopic composition in ambient air and  
250 target gas were calculated using an interpolation of the reference air analyzed  
251 before and afterwards. A custom made LabView software program (National  
252 Instruments Corp., USA) was used to control and log the temperature of the  
253 traps, the valve switching and the flow setpoints of the MFCs.

### 254 **2.3.3. IRMS system isotope calibration**

255 The isotope calibration of the IRMS system was based on a reference air cylinder  
256 that contains ambient air collected at the IMAU in 2014, with 1888 nmol/mol of  
257 CH<sub>4</sub> and isotope values of  $\delta^{13}\text{C} = (-47.89 \pm 0.05) \text{‰}$  and  $\delta\text{D} = (-88.08 \pm 1.1) \text{‰}$ .  
258 The isotope calibration scale is based on the reference scale that was described  
259 in detail in Brass and Röckmann (2010). We used the average of the reference air  
260 measurement before and after the sample air measurement to calculate the mole  
261 fraction and  $\delta$  values. The linear response of the analytical system (independence  
262 of the  $\delta$  value on the amount of CH<sub>4</sub> analyzed) was verified by injecting various  
263 volumes of reference air up to a volume equivalent to 2700 nmol/mol.  
264 Occasionally, the long-term stability of the system was checked by measuring 3  
265 target cylinders with different CH<sub>4</sub> mole fractions and isotopic compositions. A  
266 robust link of the isotopic composition to the international reference materials  
267 VPDB and VSMOW has been established in the framework of the INGOS project  
268 (Sperlich et al., 2016).

### 269 **2.4. QCLAS system**

270 The analytical procedure of the laser based measurement system involves two  
271 steps: preconcentration of the CH<sub>4</sub> from 7.5 L of ambient air in a trace gas  
272 extractor (TREX) by adsorption on HayeSep D (Eyer et al., 2014; Mohn et al.,  
273 2010) and analysis of CH<sub>4</sub> isotopologues with a modified commercial QCLAS  
274 (QCL-76-D, Aerodyne Inc., USA). Details on the development, optimization and  
275 validation of the TREX-QCLAS system are given by Eyer et al. (2015).

276 The present manuscript comprises the first application of the TREX-QCLAS  
277 system for in-situ analysis of CH<sub>4</sub> isotopologues at a field site for an extended  
278 period of time. In comparison to the original setup, the heating power of the

279 polyimide foil on the cold trap was reduced to 60 W to increase its lifetime. Due  
280 to the lower heating power, the duration of the desorption step had to be  
281 extended, which led to an improved separation from residual bulk gases (e.g. N<sub>2</sub>  
282 and O<sub>2</sub>). Lowering the O<sub>2</sub> enhancement in the gas matrix is also the main reason  
283 for a lower offset in δ<sup>13</sup>C of (1.58 ± 0.2) ‰, with respect to the MPI - scale, as  
284 compared to 2.3 ‰ in previously published results (Eyer et al., 2015). The  
285 offset was related to a higher O<sub>2</sub> mole fraction in the gas matrix after CH<sub>4</sub>  
286 preconcentration. One measurement cycle consisted of four consecutive  
287 measurements of ambient air samples and one sample of pressurized air used as  
288 a target gas, followed by a calibration phase and took around 4:30 hours. This  
289 translates into an analysis time of 54 minutes per sample of ambient or  
290 pressurized air.

291 A calibration gas (CG1, (1200 ± 50) μmol/mol CH<sub>4</sub> in high purity synthetic air  
292 (79.5% N<sub>2</sub> and 20.5% O<sub>2</sub>), δ<sup>13</sup>C = -(44.24 ± 0.10) ‰, δD = -(104.7 ± 1.1) ‰) was  
293 diluted with the same synthetic air to 688 μmol/mol and analyzed between  
294 every preconcentrated sample as an anchor to correct the measurements for  
295 instrumental drift. A second calibration gas (CG2, (1103.8 ± 3.5) μmol/mol CH<sub>4</sub>,  
296 δ<sup>13</sup>C = -(36.13 ± 0.10) ‰, δD = -(180.6 ± 1.1) ‰), diluted to a similar CH<sub>4</sub> mole  
297 fraction of 681 μmol/mol was used to calculate calibration factors for δ<sup>13</sup>C and  
298 δD values. Furthermore, gas cylinders of pressurized ambient air, referred to as  
299 target gas (TG1, TG2), were frequently measured over the entire campaign to  
300 determine and verify the repeatability of the measurement system, which was  
301 found to be 0.28 ‰ and 1.7 ‰ for δ<sup>13</sup>C and δD (1σ), respectively. Additional  
302 adjustments in the preconcentration procedure and in the analytical routine for  
303 isotope analysis improved the repeatability to 0.18 ‰ and 0.85 ‰ for δ<sup>13</sup>C and  
304 δD in the last month of the campaign. One example is the improved temperature  
305 control of the trap during adsorption, which in turn stabilized the O<sub>2</sub> content in  
306 the measuring gas and thereby reduced variations in δ<sup>13</sup>C-CH<sub>4</sub>.

307 The CH<sub>4</sub> isotopic composition of the calibration gases, as well as the target gases  
308 (pressurized air, TG1, (2639.5 ± 0.6) nmol/mol CH<sub>4</sub>, δ<sup>13</sup>C = -(46.48 ± 0.10) ‰, δD  
309 = -(119.0 ± 1.1) ‰, TG2, (2659.8 ± 0.6) nmol/mol CH<sub>4</sub>, δ<sup>13</sup>C = -(45.87 ± 0.10) ‰,  
310 δD = -(114.1 ± 1.1) ‰) were determined by the Stable Isotope Laboratory at the

311 Max-Planck-Institute for Biogeochemistry. CH<sub>4</sub> mole fraction measurements  
312 were linked to the WMO-X2004 calibration scale (Dlugokencky et al., 2005)  
313 through calibration of the target gases against NOAA reference standards at  
314 Empa.

## 315 **2.5. Modeling**

316 Two complementary atmospheric transport models (TM5, FLEXPART-COSMO),  
317 both in combination with two different emissions inventories (TNO-MACC\_2,  
318 EDGAR/LPJ-WhyMe), were applied to support interpretation of the  
319 measurements. The Eulerian tracer model TM5 simulated the distribution of CH<sub>4</sub>  
320 and <sup>13</sup>CH<sub>4</sub> at global scale with a zoom on Europe at 1° x 1° resolution and  
321 considered both the isotopic signatures of different sources and the fractionation  
322 by different removal pathways of CH<sub>4</sub> in the atmosphere. The Lagrangian particle  
323 dispersion model FLEXPART-COSMO, conversely, was run in backward mode at a  
324 higher resolution of 0.06° x 0.06° but only over Europe. This model is better able  
325 to represent the spatial variability of CH<sub>4</sub> sources in the near field of Cabauw but  
326 it only simulated the contributions from the last 4 days of emissions within  
327 Europe and not the large-scale background. Chemical loss of CH<sub>4</sub> was not  
328 considered due to the short transport times between the sources and the  
329 receptor point at Cabauw.

### 330 **2.5.1. TM5 modeling**

331 Simulations of atmospheric CH<sub>4</sub> and δ<sup>13</sup>C were performed using the global tracer  
332 model TM5 (Krol et al., 2005). The Eulerian off-line model was driven by  
333 meteorological fields from the European Centre for Medium Range Weather  
334 Forecast (ECMWF) reanalysis project ERA-Interim (Dee et al., 2011), pre-  
335 processed for use in TM5. For vertical transport due to moist convection we  
336 made use of Era Interim archived convective mass fluxes, replacing the use of the  
337 Tiedke scheme in Krol et al. (2005). The model was run at a horizontal resolution  
338 of 6°x4° globally and 1°x1° inside a zoom domain covering Western Europe. The  
339 model uses 25 hybrid sigma-pressure levels from the surface to top of  
340 atmosphere.

roeckman 1/8/2016 14:21

Deleted: Eulerian

roeckman 1/8/2016 14:23

Deleted: δD was only simulated with FLEXPART-COSMO.

344 Two parallel (forward) TM5 simulations were performed with CH<sub>4</sub> and <sup>13</sup>CH<sub>4</sub> as  
345 transported tracers. In the standard configuration, anthropogenic CH<sub>4</sub> emissions  
346 were taken from EDGAR4.2 FT2010 (EDGAR, 2009), extrapolated to 2014 and  
347 2015 using annual statistics from the Food and Agriculture Organization of the  
348 United Nations (FAO) and the British Petroleum Company (BP), as described in  
349 Houweling et al. (2014). For natural wetland emissions, an average of the  
350 emission estimates derived by Spahni et al. (2011) for the period 2003-2008 was  
351 taken, using the LPJ-WhyMe model. For a complete description of the CH<sub>4</sub>  
352 emissions (Table 1), see Monteil et al. (2013) and references therein. <sup>13</sup>CH<sub>4</sub>  
353 emissions were derived from the CH<sub>4</sub> emissions using prescribed δ<sup>13</sup>C source  
354 signatures (Table 1). The emission inventory was built according to a double  
355 constraint: 1<sup>st</sup>, each source signature must be chosen within its own uncertainty  
356 interval, and 2<sup>nd</sup>, the resulting global average source signature must be  
357 compatible with the global source signature that is inferred from the  
358 observations (and that is known with a much better precision than the individual  
359 source signatures) (Monteil et al., 2011). In a second set of simulations,  
360 anthropogenic emissions in a regional domain centered on Cabauw were  
361 replaced by emissions from the European TNO-MACC\_2 inventory, which was  
362 used as the standard inventory in the FLEXPART-COSMO simulations (see  
363 below). Outside the regional domain covered by TNO-MACC\_2, the EDGAR  
364 emissions were used.

365 Atmospheric removal of CH<sub>4</sub> was modeled as described in Monteil et al. (2013),  
366 using kinetic fractionation factors  $\alpha = k(^{12}\text{C}) / k(^{13}\text{C})$  of  $\alpha_{\text{OH}} = 1.0055$ ,  $\alpha_{\text{Cl}} = 1.066$   
367 and  $\alpha_{\text{O}(^1\text{D})} = 1.013$  for the reactions between CH<sub>4</sub> and OH (Sander et al., 2006), Cl  
368 (Saueressig et al., 1995) and O(<sup>1</sup>D) (Saueressig et al., 2000), respectively. The  
369 simulations were initialized at steady state (obtained via a spin-up run) in 2005,  
370 and simulations of the period 2005-2015 were used to calculate a realistic state  
371 of the atmosphere at the start of the measurement campaigns, including the  
372 imbalance between emissions and atmospheric CH<sub>4</sub> mixing ratio/isotopic  
373 composition in 2014. Time series were extracted from model-simulated mole  
374 fraction fields after interpolation to the horizontal coordinate and height of the  
375 Cabauw tower air inlet.

roeckman 1/8/2016 14:24

Formatted: Font:Not Italic, Underline

376 **2.5.2. FLEXPART-COSMO modeling**

377 The Lagrangian Particle Dispersion Model (LPDM) FLEXPART (Stohl et al., 2005)  
378 was used in a modified version coupled to the mesoscale numerical weather  
379 forecast model COSMO (Baldauf et al., 2011) to simulate the regional  
380 contribution of different source categories to the concentrations and isotopic  
381 signatures of CH<sub>4</sub> at Cabauw. FLEXPART-COSMO was driven by hourly  
382 operational analysis fields generated by the Swiss national weather service  
383 MeteoSwiss for a domain covering entire western and central Europe from  
384 Ireland, Denmark, and Poland in the north to Portugal and southern Italy in the  
385 south with a horizontal resolution of approximately 7 km x 7 km and 60 vertical  
386 levels. Every 3 hours, 50'000 particles (air parcels) were released from the  
387 position of the inlet 20 m above surface and traced backward in time for 4 days  
388 to compute the sensitivity of each 3-hourly measurement to upwind sources. The  
389 corresponding source sensitivity maps or footprints (Seibert and Frank, 2004)  
390 were multiplied with gridded CH<sub>4</sub> emissions to compute the mole fraction  
391 enhancement above background expected from different sources. Emissions  
392 were taken from the TNO-MACC\_2 inventory for Europe representative of the  
393 year 2009 and available at 0.125° x 0.0625° resolution (Kuenen et al., 2014) or,  
394 alternatively, from the same version of EDGAR/LPJ-WhyMe inventory driving  
395 TM5 at a resolution of 1° x 1°. Methane mole fractions were computed separately  
396 for a number of SNAP (Standardized Nomenclature for Air Pollutants) source  
397 categories with specific isotopic signatures as summarized in Table 2.

398 For the domain covered by the FLEXPART-COSMO simulations, which includes  
399 most of western and central Europe, total anthropogenic emissions are 20.6 Tg  
400 CH<sub>4</sub>/yr in EDGAR and 18.3 Tg CH<sub>4</sub>/yr in TNO-MACC, which corresponds to a  
401 difference of 12.5%. CH<sub>4</sub> emissions from gas/oil production and distribution are  
402 89% higher, CH<sub>4</sub> emissions from agriculture 19% lower and CH<sub>4</sub> emissions from  
403 waste 12% higher in EDGAR than in TNO-MACC.

404 Source specific emissions were combined with isotopic signatures of the various  
405 categories from Table 2 to derive mean δ<sup>13</sup>C and δD isotopic signatures for the  
406 CH<sub>4</sub> that was picked up by the air parcel along the trajectory.

407 **2.6. Interpretation of CH<sub>4</sub> isotope data**

### 408            **2.6.1. Data analysis by a Keeling plot technique**

409    The isotopic composition of CH<sub>4</sub> emissions were estimated using the Keeling plot  
410    technique (Keeling, 1961; Pataki et al., 2003). This method allows the isotopic  
411    signature of a single source process or the mean isotopic signature of combined  
412    source processes that mix into a background reservoir to be determined from  
413    the observed ambient isotopic composition and mole fraction. An implicit  
414    assumption of the Keeling plot approach is that the isotopic composition and  
415    mole fraction of the background reservoir and the isotopic composition of the  
416    source or the combined source stay constant over the time range of the analysis.  
417    This may not always apply as the relative contribution of individual CH<sub>4</sub> sources  
418    or their isotopic signature may change over time

419    To exploit the high temporal resolution of our data, we applied a novel approach  
420    of a moving Keeling plot (MKP) method. Data within a moving window of 12  
421    hours were used to calculate the source isotopic composition. This window was  
422    moved in 1-hour time steps over the data series. In addition, values for  
423    background conditions within a 48-hour period, centered on the respective 12-  
424    hour window, were included in the analysis. These background values were  
425    chosen between 10:00 and 18:00 local time, because during this period a  
426    convective boundary layer usually develops and hence local influence is weak;  
427    pollution events with CH<sub>4</sub> mole fractions above 2100 nmol/mol were filtered out  
428    additionally. For each time window, an orthogonal least squares fit was applied  
429    to the  $\delta$  values vs. the inverse CH<sub>4</sub> mole fractions and R<sup>2</sup> values were calculated.  
430    A Keeling plot analysis only returns meaningful values for the source isotopic  
431    composition if the variations in CH<sub>4</sub> mole fraction are significant and if the  
432    emissions are from a source with a well-defined isotopic composition. Therefore,  
433    two additional filters were applied: i) the mole fraction had to vary by more than  
434    200 nmol/mol within each time window and ii) the R<sup>2</sup> of the fit had to be larger  
435    than 0.8. If R<sup>2</sup> < 0.8, the 12 h interval was reduced consecutively by one hour to a  
436    minimum of six hours until either the R<sup>2</sup> of the fit was > 0.8 or the number of  
437    data points was lower than five. On average this technique accumulated 22 data  
438    points per 12-h time window.

### 439    **3. Results**



### 440 3.1. Overview of the field measurements at the Cabauw site

441 The full record of the methane mole fraction and isotopic composition obtained  
442 with the two measurement techniques at the CESAR site is shown in Fig. 2. The  
443 IRMS system started with  $\delta D$  measurements first, and after 3 weeks delivered  
444 both  $\delta^{13}C$  and  $\delta D$  data. The TREX-QCLAS system started later and ran  
445 continuously from mid-December to mid-January, and from mid-February to the  
446 end of the campaign. Despite a number of interruptions mainly due to various  
447 kinds of instrument malfunction, the combined time series of both techniques  
448 shows a high temporal coverage with more than 2500 measurements performed  
449 for both  $\delta^{13}C$  and  $\delta D$ .

450 A qualitative inspection of the time series already conveys the obvious features  
451 that will be discussed below in more detail: the methane mole fraction  $\chi(CH_4)$   
452 shows a large number of substantial increases above background level, and these  
453 positive methane excursions are accompanied by negative excursions in the  $\delta$   
454 values from the background level. Thus the additional methane is generally  
455 depleted in both  $^{13}C$  and D.

### 456 3.2. Comparison of the two analytical techniques

457 Before presenting a detailed analysis of the  $CH_4$  isotopic composition in ambient  
458 air, we compare the results obtained with the IRMS and QCLAS techniques in  
459 order to evaluate their performance and to combine the results into one final  
460 dataset. Although both systems measured air from the same intake line, the  
461 sampling intervals could not be synchronized since both instruments operated in  
462 different measurement cycles. A full measurement cycle (including measurement  
463 of the reference gas) took 84 minutes for the IRMS system and 54 minutes for  
464 the TREX-QCLAS system. The actual duration of the air sampling was 10 minutes  
465 for the IRMS system and 15 minutes for the QCLAS system. So even if the systems  
466 coincidentally started sampling at the same time, they never actually analyzed  
467 exactly the same air mass. Consequently, differences between the systems  
468 contain contributions from natural variability, random fluctuations due to  
469 limited measurement precision, and system offsets.

470 Fig. 3 shows a comparison of the  $\chi(CH_4)$ , as well as  $\delta^{13}C$  and  $\delta D$  values that were  
471 obtained with the TREX-QCLAS and the IRMS technique. To visualize the possible

roeckman 1/8/2016 14:25

Deleted: Inter-c

473 effect of time shifts, the size of the points corresponds to the proximity of the  
474 sampling intervals. A total of 727, 333 and 277 measurement pairs for  $\chi(\text{CH}_4)$ ,  
475  $\delta^{13}\text{C}$  and  $\delta\text{D}$ , respectively, analyzed by both techniques were combined in this  
476 way.

477 The mole fraction comparison shows good agreement along the 1:1 line but with  
478 a large scatter, which has two contributions: i) instrumental noise, as the isotope  
479 systems have a relatively large uncertainty for measurement of the mole fraction  
480 compared to existing high-precision  $\text{CH}_4$  analyzers, and ii) natural variability  
481 associated with the sampling of different air masses as described above. The  
482 second point is supported by the fact that the average difference in  $\text{CH}_4$  mole  
483 fractions between the two analytical techniques was larger for larger temporal  
484 differences in the sampling intervals.

485 For the isotope intercalibration plots, the grey-black shading of the circles  
486 indicates the difference in  $\chi(\text{CH}_4)$  of the respective measurement pair analyzed  
487 by both techniques. The overall difference between the measurements  
488 conducted with the two systems (QCLAS-IRMS) is  $(+0.25 \pm 0.04) \text{‰}$  for  $\delta^{13}\text{C}$  and  
489  $(-4.3 \pm 0.4) \text{‰}$  for  $\delta\text{D}$  (the stated errors are standard errors of the mean). The  
490 mean offsets are slightly outside the WMO extended compatibility goals for  $\delta^{13}\text{C}$   
491 ( $0.2 \text{‰}$ ) and within the WMO extended compatibility goals for  $\delta\text{D}$  ( $5 \text{‰}$ ), as  
492 indicated by the red dashed lines (WMO, 2014). Individual measurement pairs  
493 can show significantly larger deviations for aforementioned reasons. Differences  
494 between the two techniques are higher than expected as both laboratories refer  
495 their measurements to MPI-BGC, who recently established a link between the  
496  $\text{CH}_4$  isotopic composition and the international reference materials VPDB and  
497 VSMOW, in the framework of the INGOS project (Sperlich et al., 2016). Therefore,  
498 remaining differences can only be rationalized by uncertainties in propagating  
499 the scale or by instrumental issues. The enhanced discrepancies for low  $\delta\text{D}-\text{CH}_4$   
500 values might originate from a non-linear response of one of the applied  
501 analytical techniques. The mean offset values determined above were applied to  
502 the QCLAS data to create one combined dataset with 2610 data points for  $\delta^{13}\text{C}$   
503 and 2673 data points for  $\delta\text{D}$ .

### 504 **3.3. FLEXPART-COSMO source attribution**

505 In FLEXPART-COSMO, the contributions of the individual source types are  
506 simulated separately and added up to obtain the cumulative CH<sub>4</sub> mole fraction.  
507 Fig. 4 shows these contributions in absolute (top) and relative terms (bottom).  
508 According to the model, the relative contributions at the Cabauw site are quite  
509 uniform, with agricultural sources accounting for more than 60%, waste (mostly  
510 landfills) around 20–40%, and fossil sources between 0 and 40%. We note that  
511 significant contributions from fossil sources are only detected episodically,  
512 during several events that usually last a few days. Contributions from other  
513 source categories are generally negligible at the Cabauw site.

#### 514 **3.4. TM5 and FLEXPART-COSMO modeling including isotopes**

515 The TM5 model calculates the combined influence of the global methane sources  
516 and sinks on CH<sub>4</sub> and δ<sup>13</sup>C at the Cabauw tower, and therefore the TM5 results  
517 can be compared directly to the measured time series. For FLEXPART-COSMO, a  
518 representative background mole fraction and isotopic signature needs to be  
519 added for comparison with the observations. For simplicity we assumed a  
520 constant background similar to the observed values for background conditions:  
521 1930 nmol/mol for χ(CH<sub>4</sub>) with δ<sup>13</sup>C = -47.1 ‰ and δD = -86 ‰.

522 Fig. 5 shows a comparison of these model-generated time series with the  
523 measured data for the entire campaign. Both models capture the amplitude and  
524 the temporal variability of χ(CH<sub>4</sub>)<sub>well</sub>. Most of the methane pollution events  
525 observed at the CESAR site are also present in the modeled time series and the  
526 increase in χ(CH<sub>4</sub>) is of a comparable size. In addition, the results of the TM5 and  
527 the FLEXPART-COSMO model for CH<sub>4</sub> mole fractions agree relatively well with  
528 each other (R<sup>2</sup>=0.69), in particular when both models are run with the same  
529 inventory at the same coarse spatial resolution, i.e. with EDGAR/LPJ-WhyMe.

530 A few pronounced CH<sub>4</sub> events in Fig. 5 show larger differences between the  
531 models. On 2 November, FLEXPART-COSMO simulates an emission signal that is  
532 not captured by TM5. Unfortunately no measurements are available for this  
533 event to decide on which model performs better. On 30 November TM5  
534 simulates a CH<sub>4</sub> plume, which is absent in FLEXPART-COSMO, and this event is  
535 also not supported by the measurements. The global model has the advantage

536 that it includes the influence of long-range transport. As expected, however, the  
537 observed variability is predominantly influenced by local and regional emissions.  
538 Regarding the time series of the  $\delta$  values, both TM5 and FLEXPART-COSMO  
539 qualitatively display the expected anti-correlations between  $\text{CH}_4$  and  $\delta^{13}\text{C}$ .  
540 However, the amplitude of the  $\delta^{13}\text{C}$  variability is generally underestimated in the  
541 model runs, especially when using the EDGAR inventory. In addition, the  
542 modeled background level of  $\delta^{13}\text{C}$  in TM5 is offset by up to 1 ‰, but this offset is  
543 also present at clean background sites in the Northern hemisphere.

544 Using the TNO-MACC inventory in FLEXPART-COSMO results in better  
545 agreement with the observed variability of  $\delta^{13}\text{C}$ . In TM5, the TNO-MACC  
546 emissions reduce the amplitude of the  $\text{CH}_4$  variability, which is explained by the  
547 13% lower emissions in TNO-MACC compared with EDGAR. Furthermore, the  
548 results of both models are consistent with the emissions being more depleted in  
549  $\delta^{13}\text{C}$  in TNO-MACC than in EDGAR. The measurements indicate emissions that  
550 are even more depleted in  $\delta^{13}\text{C}$  than TNO-MACC values. These results suggest  
551 that the fractional contribution of isotopically heavy fossil emissions is  
552 overestimated in EDGAR, at least in the area sampled by Cabauw, although the  
553 uncertainty in the assumed  $\delta^{13}\text{C}$  source signatures could also contribute. For  
554 instance, recent literature showed that landfill emissions from the UK are more  
555 depleted in  $^{13}\text{CH}_4$  due to the implementation of gas extraction systems (Zazzeri  
556 et al., 2015).

557 The  $\delta\text{D}$  time series simulated with FLEXPART-COSMO using the TNO-MACC  
558 inventory is in good agreement with the measurements. This further indicates  
559 that TNO-MACC has a realistic source mixture, but the uncertainties in the mean  
560  $\delta\text{D}$  signature are too large to draw firm conclusions at this stage. Despite these  
561 uncertainties, Fig. 5 clearly demonstrates how isotopic measurements highlight  
562 differences between emission inventories, which would go unnoticed looking  
563 only at  $\text{CH}_4$  mole fractions. Additional information may be available from the  
564 combination of both isotope signatures. For several of the  $\text{CH}_4$  elevation events  
565 shown in Fig. 5b, the relative changes in  $\delta^{13}\text{C}$  and  $\delta\text{D}$  modeled with FLEXPART-  
566 COSMO vary when using the two different inventories (TNO-MACC and EDGAR).  
567 Some of the anomalies show differences pointing in the same direction for  $\delta^{13}\text{C}$

568 and  $\delta D$ , and some others not. This suggests that  $\delta D$  provides additional  
569 independent information, which will be discussed in more detail in Section 4.3  
570 using a double isotope plot of the source signatures (Fig. 7). The benefit of the  
571 high-resolution dual isotope measurements for validating emissions used in the  
572 models will be investigated in Section 4.4.

## 573 **4. Discussion**

### 574 **4.1. Diurnal and synoptic variability**

575 A prominent feature of the high-resolution dataset is the pronounced diurnal  
576 variability, with large increases in  $CH_4$  mole fraction that occur often during the  
577 night, due to the shallow planetary boundary layer. In addition, there are also  
578 several synoptic (but much smaller) pollution events, where  $CH_4$  mole fractions  
579 stay above the unpolluted background level for several days. These elevations  
580 are likely caused by synoptic scale advection of  $CH_4$  plumes from other source  
581 regions with a different source mix.

### 582 **4.2. Isotope identification of the mean $CH_4$ source**

583 In Fig. 6, the Keeling plot technique is applied to identify the mean isotopic  
584 signatures ( $\delta^{13}C$ ,  $\delta D$ ) of the combined  $CH_4$  emissions detected at the Cabauw site.  
585 An orthogonal regression method was applied to determine the fit parameters.  
586 This analysis yields well-defined mean isotopic signatures of the cumulative  
587 source (the y-intercept of the regression analysis) of  $\delta^{13}C = -(60.8 \pm 0.2) \text{‰}$  and  
588  $\delta D = -(298 \pm 1) \text{‰}$ . The inferred mean isotopic signature agrees well with  
589 emission from ruminants, which are expected to be the main source of  $CH_4$  in  
590 this rural area. This is plausible, because the mean isotopic signature is largely  
591 determined by the pronounced nighttime  $CH_4$  elevations, which represent the  
592 local emissions close to the tower. Also the source contributions modeled by  
593 FLEXPART-COSMO suggest the dominant influence of agricultural emissions in  
594 this rural area (Fig. 4). Interestingly, the mean isotopic signature for the much  
595 smaller synoptic  $CH_4$  variations of the background (red points in Fig. 6) is not  
596 significantly different from the one for the complete dataset.

### 597 **4.3. Short-term variability**

598 Given the high temporal resolution of the dataset presented here, the isotope  
599 variations can be interpreted in much more detail than the overall analysis  
600 performed above. This allows identifying varying contributions of CH<sub>4</sub> sources  
601 during different periods of the campaign. To do so, we applied a 12-hour Moving  
602 Keeling Plot (MKP) method to the data, as described in Sect 2.6.1.

603 Fig. 7 summarizes the results of the MKP method in the form of a  $\delta D$  vs.  $\delta^{13}C$  plot.  
604 To combine  $\delta^{13}C$  and  $\delta D$  measurements performed at different times, MKP  
605 intercepts were averaged over 6 h intervals. Mean  $\delta^{13}C$  signatures range between  
606 -68 ‰ and -55 ‰ and mean  $\delta D$  signatures cover a relatively wide range  
607 between -350 ‰ and -260 ‰, indicating emissions mainly from microbial  
608 sources as derived from the cumulative Keeling plot analysis. During some  
609 periods, however, elevated mean  $\delta^{13}C$  and  $\delta D$  signatures reveal significant  
610 additional contributions from waste and/or fossil emissions.

611 The colored symbols in Fig. 7 highlight the mean isotopic signatures of three 48 h  
612 events (10-12, 16-18 and 22-24 March) that are discussed in more detail in the  
613 following. For the event of 16-18 March, selected results of the 12 h MKP method  
614 are displayed in Fig. 8, demonstrating the advantage of the high temporal  
615 resolution data. It is possible to clearly distinguish variations in the mean  
616 isotopic signatures during this event by variations in the y-axis intercepts. The  
617 increase by about 6 ‰ for  $\delta^{13}C$  and about 50 ‰ for  $\delta D$ , in the source isotopic  
618 signature for this event, clearly indicates the gradually increasing contribution of  
619 CH<sub>4</sub> from isotopically enriched sources, e.g. fossil fuel- or waste-related CH<sub>4</sub>.

620 The temporal evolution of the observed source mixture is investigated in further  
621 detail in Fig. 9, where the 16-18 March period (labeled as 2) is compared to two  
622 other 48 h – periods (10-12 March; label 1, and 22-24 March; label 3), each with  
623 significant diurnal CH<sub>4</sub> elevations. For event 1, the mean isotopic signatures  
624 stayed rather constant at values around  $\delta^{13}C = -63$  ‰ and  $\delta D = -320$  ‰. These  
625 values are typical for microbial emissions from an agricultural source and agree  
626 well with the source contributions predicted for this period by the FLEXPART-  
627 COSMO model.

628 Period 2 is characterized by much stronger isotopic change within the 48 h  
629 period. The  $\delta^{13}C$  signature increases to above -60 ‰ and the  $\delta D$  signature

630 increases to -240 ‰ by the end of the period (see Fig. 9). The double-isotope  
631 plot in Fig. 7 shows that the change in  $\delta D$  during event 2b clearly points towards  
632 fossil fuel sources, which provides independent support for the FLEXPART-  
633 COSMO simulations, where the contributions from fossil-fuel- derived emissions  
634 are higher for the second day.

635 For period 3, the mean  $\delta^{13}C$  isotopic signatures increased during the 48 h by  
636 about 2-3 ‰, whereas the  $\delta D$  signatures remained constant around -300 ‰. For  
637 this period, the double isotope plot of Fig. 7 indeed shows a shift towards the  
638 waste category. Also this observation is independently confirmed (at least  
639 qualitatively) by the FLEXPART-COSMO model derived source attribution, which  
640 indicates the largest fraction of waste-derived  $CH_4$  for the first day and a small  
641 addition of fossil  $CH_4$  for the second day of event 3. These examples show that  
642 even at a location like Cabauw, where one source category strongly dominates,  
643 contributions from isotopically different sources can be identified if sufficiently  
644 high-resolution dual isotope ratio data are available. We note that the  
645 “directional” information in the double isotope plot is only available by  
646 combining  $\delta^{13}C$  and  $\delta D$  measurements. It would be much harder, if not  
647 impossible, to detect an addition from fossil fuel- or landfill- derived  $CH_4$  based  
648 on  $\delta^{13}C$  or  $\delta D$  data alone.

#### 649 **4.4. Evaluation of emission databases with high temporal resolution $CH_4$** 650 **isotope data**

651 As described in Section 3.4, both the TM5 and the FLEXPART-COSMO model-  
652 generated time series of  $CH_4$  mole fractions show an adequate agreement with  
653 the  $CH_4$  measurements at the Cabauw site. Therefore, the comparison between  
654 measurement data and the models can be used to evaluate the methane budget  
655 in more detail. In this context, the measured and modeled isotopic composition  
656 can be employed to assess the validity of emission inventories, EDGAR and TNO-  
657 MACC, with respect to the magnitude and spatial distribution of source  
658 categories. To compare the measured mean isotopic signatures to the model  
659 results, the simulated isotope time series were linearly interpolated and  
660 evaluated in the same way as the observations using the 12 h MKP method. This  
661 analysis was performed for both models (TM5 and FLEXPART-COSMO), each

662 using both the EDGAR/LPJ-Why-Me and the TNO\_MACC inventories.  
663 Additionally, time series for the mean isotopic signatures were calculated  
664 directly from FLEXPART-COSMO data, without using of the MKP method. This  
665 direct method allowed an independent estimation of the mean isotopic  
666 signatures and, thus, also provided an opportunity to evaluate the MKP method.

667 The statistics of the mean isotopic signatures from all four model-inventory  
668 combinations are shown as histograms in Fig. 10, together with the  
669 measurement-derived mean isotopic signatures and the directly derived  
670 signatures from FLEXPART-COSMO modeling. A clear difference can be observed  
671 between the mean isotopic signatures derived with the two different emission  
672 inventories. Model runs with the EDGAR/LPJ-WhyMe emission inventory (red in  
673 Fig. 10) tend to produce mean CH<sub>4</sub> isotopic signatures that are more enriched in  
674 <sup>13</sup>C and D than the model runs with TNO-MACC emissions. These differences are  
675 very similar for the simulations using TM5 and FLEXPART-COSMO, suggesting  
676 that differences originate from the emission inventories, rather than from  
677 differences between the models themselves. The δ<sup>13</sup>C source signatures derived  
678 from the measurements at the Cabauw tower are significantly more depleted  
679 than any of the model-generated datasets. For δD, the mean isotopic signatures  
680 using TNO-MACC emissions are relatively close to the measurements at Cabauw,  
681 whereas the values using EDGAR emissions are much more enriched in CH<sub>3</sub>D.

682 The high temporal resolution isotope data that are described in this paper thus  
683 provide relevant information to further constrain models and/or emission  
684 inventories, because the mean isotopic signatures can change rapidly. The  
685 comparison of our first high-resolution isotope measurements at Cabauw to  
686 model calculations clearly identify differences between the modeled inventories,  
687 where the EDGAR inventory produced too enriched mean isotopic signatures  
688 due to a higher contribution from fossil fuel sources. Similar differences in terms  
689 of source contributions between EDGAR and TNO-MACC\_2 were also reported by  
690 Hiller et al. (2014) for Switzerland, and Henne et al. (2015) concluded that  
691 natural gas emissions in Switzerland are likely overestimated in EDGAR.

## 692 **5. Conclusions and outlook**



693 The dual isotopic composition of CH<sub>4</sub> has been monitored for the first time with  
694 high temporal resolution in an extended (5 months) field deployment with two  
695 different instruments, an IRMS system and a QCLAS system, at the tall tower site  
696 Cabauw, the Netherlands. The measurements of both instruments compare well  
697 and can be combined to a time series of more than 2500 measurements for both  
698 δ<sup>13</sup>C and δD. Using a moving Keeling plot technique, the mean isotopic signatures  
699 of periods with significant CH<sub>4</sub> elevations can be derived with high temporal  
700 resolution. The combination of δ<sup>13</sup>C and δD data provides strong constraints to  
701 distinguish emissions from different source categories. Overall, CH<sub>4</sub> emissions at  
702 the Cabauw tall tower are dominated by agricultural sources, but variations in  
703 the mean isotopic signatures allow identification of events with increased  
704 contributions from fossil fuel and waste sources, which can be used to validate  
705 variations in the source mix, calculated using the FLEXPART-COSMO model.

706 The high-resolution isotope ratio measurements at Cabauw were compared to  
707 model calculations that used two different emission inventories. When two very  
708 different models (TM5 and FLEXPART-COSMO) used emissions from the EDGAR  
709 inventory, they produced clearly too enriched mean isotopic signatures. The  
710 modeled mean isotopic signatures were systematically more depleted and closer  
711 to the measured ones when the TNO-MACC inventory was used. The differences  
712 in the source signatures appear to originate from differences in the inventories  
713 and not from differences in the models, which supports indications in the recent  
714 literature that fossil fuel related emissions might be overestimated in EDGAR. We  
715 note that measurements at Cabauw reflect only one limited region of the  
716 European domain, and given the many degrees of freedom (transport, source  
717 signatures used in the models, emission inventories), one single dataset is not  
718 sufficient to make a final decision on the quality of the emission dataset. High  
719 frequency analysis of δ<sup>13</sup>C- and δD at several locations would allow better  
720 constraints on isotope source signatures and emissions in atmospheric models.  
721 Our proof-of-concept study presented here using continuous high-resolution  
722 techniques shows that this will be feasible in the future.

723

724 | [Data availability](#)

725 [The data used for the scientific analysis of this paper are available as](https://www.projects.science.uu.nl/atmosphereclimate/Data.php)  
726 [supplementary information to this paper and at](https://www.projects.science.uu.nl/atmosphereclimate/Data.php)  
727 [https://www.projects.science.uu.nl/atmosphereclimate/Data.php.](https://www.projects.science.uu.nl/atmosphereclimate/Data.php)

728

### 729 **Acknowledgements**

730 This project was funded by the European Community's Seventh Framework  
731 Program (FP7/2007-2013) within the InGOS project under grant agreement No.  
732 284274. Additional funding from the Swiss National Science Foundation (SNSF)  
733 within grant No. 200021\_134611 and TNA grants within INGOS is gratefully  
734 acknowledged. The campaign at the Cabauw tall tower was made possible with  
735 strong support from Marcel Brinkenberg (KNMI), Michel Bolder and Henk  
736 Snellen (IMAU). We also thank Marco Weber (Empa) for assistance during  
737 transport and setup of the TREX-QCLAS system at the CESAR site.

### 738 **Author contributions**

739 S.E. and C.vdV. carried out the isotope measurements at the Cabauw tower.  
740 C.vdV., T.R. and W.A.B. developed the IRMS system. S.E., B.T., L.E. and J.M.  
741 developed the TREX-QCLAS system. C.vdV., S.E., J.M., T.R., B.T., M.E.P., G.Z., D.L.,  
742 E.G.N., and J.M.N. contributed to the Cabauw measurement campaign. G.M., S.H.  
743 and D.B. performed the modeling with TM5 and FLEXPART-COSMO. S.E., T.R.,  
744 J.M., B.T., E.H., D.B., G.M., S.H., C.vdV., M.E.P. and H.F. performed and contributed  
745 to the data evaluation. S.E. produced the figures for the manuscript. T.R., S.E. and  
746 J.M. wrote the manuscript with input from C.vdV., G.M., S.H., E.H., D.B., H.F. and  
747 L.E. T.R., L.E. and J.M. designed the study as part of the INGOS project.

748 **Table 1** European CH<sub>4</sub> emissions and isotope source signatures ( $\delta^{13}\text{C}$ ,  $\delta\text{D}$ ) for the  
 749 different source categories used in TM5.

Process	Yearly emissions (Europe, Tg CH <sub>4</sub> /yr)	source signature $\delta^{13}\text{C}/\text{‰}$
<b>Natural emissions</b>	<b>22.1</b>	<b>-59.2</b>
Natural wetlands (1)		
<i>Peatland</i>	9.3	-68
<i>Wet mineral soils</i>	4.6	-65
<i>Inundated wetlands</i>	1.3	-60
Geological emissions (2)	6.5	-42
Termites (3)	0.4	-63
<b>Anthropogenic emissions</b>	<b>45.3</b>	<b>-52.4</b>
Biomass burning (4)	0,3	-23.6
Agriculture (5)		
<i>Domestic ruminants</i>	11	-64
<i>Manure</i>	3	-54
<i>Rice paddies</i>	0.17	-65
Energy sector (5)		
<i>Coal mining</i>	3.4	-47
<i>Oil production</i>	3	-42
<i>Gas production and distribution</i>	12	-42
<i>Oil combustion</i>	0.41	-32
Residential sector (5)	1.6	-32
Waste treatment (5)		
<i>Landfills</i>	9	-54
<i>Waste waters</i>	3	-50
<b>Total</b>	<b>67.4</b>	<b>-54.6</b>

750 (1) Spahni et al. (2011); (2) Etiope et al. (2008); (3) Sanderson et al. (1996); (4)

751 GFED3/4 (<http://www.globalfiredata.org/>); (5) EDGAR4.2FT (EDGAR, 2010).

752

753 **Table 2** SNAP (Standardized Nomenclature for Air Pollutants) source categories  
 754 and corresponding  $\delta^{13}\text{C}$  and  $\delta\text{D}$  source signatures from the TNO-MACC\_2  
 755 inventory as used in FLEXPART-COSMO.

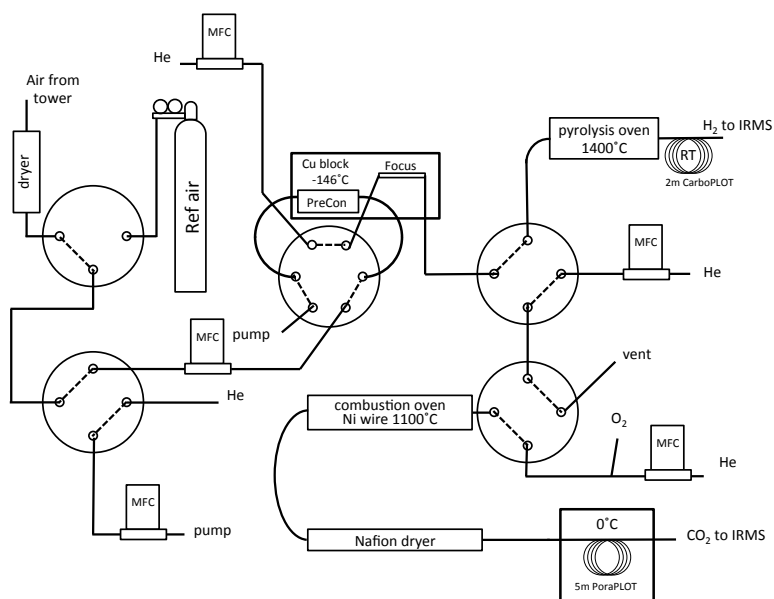
SNAP Category	Description	$\delta^{13}\text{C}/\text{‰}$	$\delta\text{D}/\text{‰}$
1	Energy industries, oil or gas production	-42	-175
2	Residential combustion	-32	-175
3+4	Industrial combustion and non-combustion processes	-60	-175
5	Extraction and distribution of fossil fuels including distribution of natural gas	-42	-175
7	Road transport	-20	-175
9	Waste including emissions from landfills	-54	-293
10	Agriculture including emissions from ruminants and manure management	-64	-319
6+8	Other emissions (negligible)	-42	-175

756

757 **Table 3.** Mean value and standard deviation of the histograms of the source  
758 isotopic composition shown in Fig. 10.

<b>Model + Inventory</b>	<b>Method</b>	<b><math>\delta^{13}\text{C}/\text{‰}</math></b>	<b><math>\delta\text{D}/\text{‰}</math></b>
Measurement data	MKP	$-61.0 \pm 2.8$	$-300 \pm 22$
TM5 + Edgar	MKP	$-53.3 \pm 1.1$	
FLEXPART-COSMO + Edgar	MKP	$-54.5 \pm 1.6$	$-277 \pm 10$
FLEXPART-COSMO + Edgar	Direct	$-53.4 \pm 1.7$	$-269 \pm 10$
TM5 + TNO-MACC	MKP	$-56.7 \pm 0.8$	
FLEXPART-COSMO + TNO-MACC	MKP	$-57.6 \pm 1.9$	$-294 \pm 12$
FLEXPART-COSMO + TNO-MACC	Direct	$-57.2 \pm 1.7$	$-289 \pm 11$

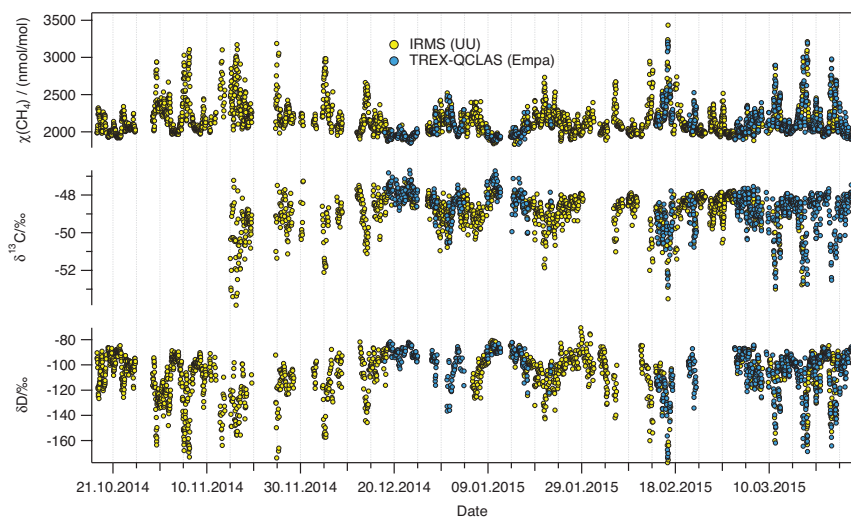
759



761 Fig. 1: Schematics of the pre-concentration and extraction system developed for  
 762 the IRMS technique. MFC denotes mass flow controller. The 8-port valve through  
 763 which the Ref air bottle was connected to the first selection valve is not shown to  
 764 reduce complexity. For further description see the main text.

765

766

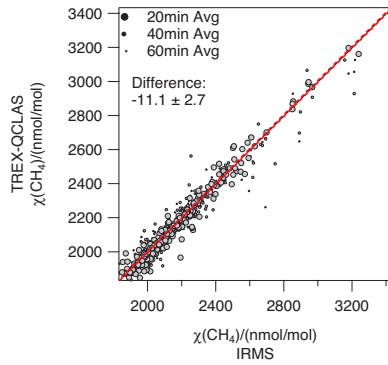


768

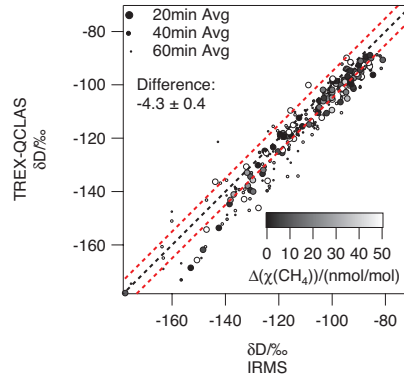
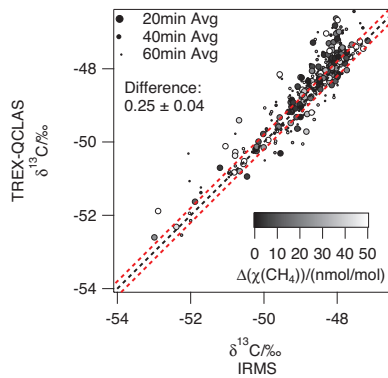
769 Fig. 2.: CH<sub>4</sub> mole fraction,  $\chi(\text{CH}_4)$ , and isotopic composition ( $\delta^{13}\text{C}$ ,  $\delta\text{D}$ ) measured  
770 at the Cabauw tall tower from 17 October 2014 until 29 March 2015. Real-time  
771 measurements by IRMS (Utrecht University) are indicated in yellow, TREX-  
772 QCLAS (Empa) data in blue.

773

774



775



776

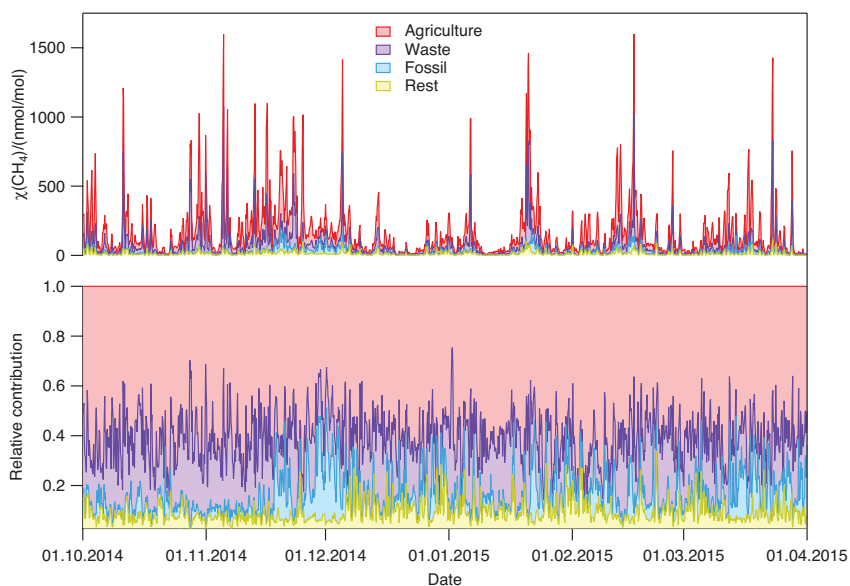
777

778

779 Fig. 3: Correlation diagrams for CH<sub>4</sub> mole fraction, δ<sup>13</sup>C and δD analyzed with  
780 IRMS (Utrecht University) and TREX-QCLAS (Empa). The dashed black lines are  
781 1:1 lines, dashed red lines mark the extended WMO compatibility goals of ± 5  
782 nmol/mol, ± 0.2 ‰ and ± 5 ‰ for CH<sub>4</sub> mole fraction, δ<sup>13</sup>C and δD, respectively.  
783 The temporal difference between IRMS and TREX-QCLAS sampling is indicated  
784 by the point size (large: 20 min, medium: 40 min, small: 60 min). For δ<sup>13</sup>C and δD,  
785 the differences in the CH<sub>4</sub> mole fraction of the measurements are represented by  
786 the shading (black: identical mole fractions, white: 50 nmol/mol difference).

787

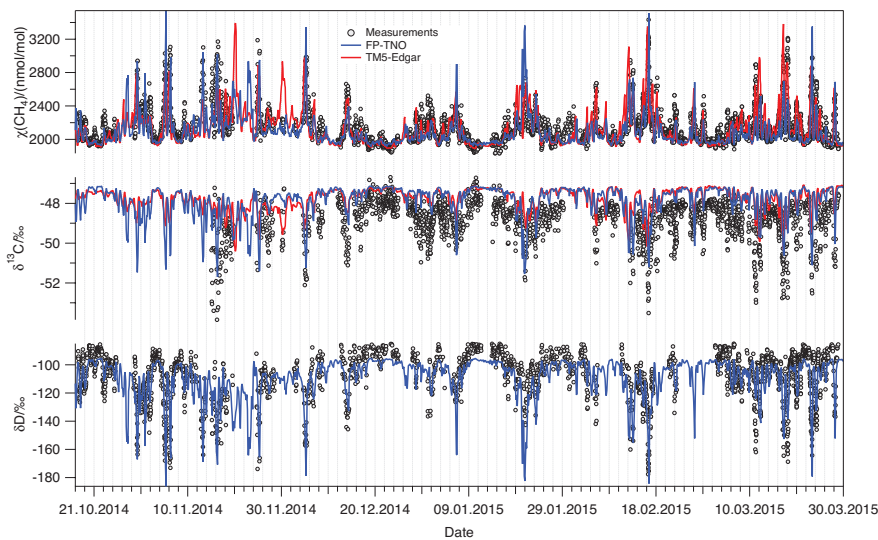




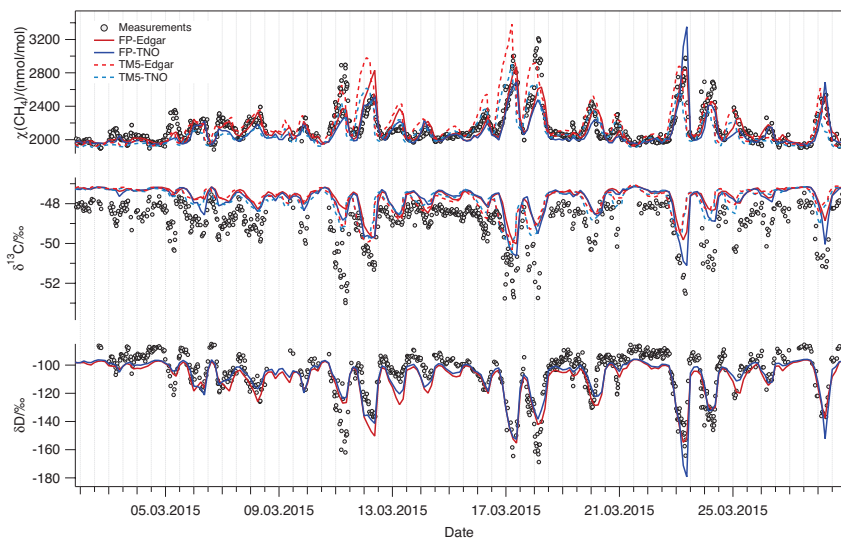
788

789 Fig. 4: Absolute (top) and relative (bottom) contributions of methane emissions  
 790 that are picked up along the 4-day FLEXPART-COSMO trajectories during the  
 791 campaign. The results shown are from the FLEXPART-COSMO simulations with  
 792 the TNO-MACC inventory. They indicate major contributions of the following  
 793 source categories: “agriculture” (mainly ruminants), “waste” (mainly landfills)  
 794 and “fossil” (fugitive losses from coal, oil and natural gas production and from  
 795 gas transportation and distribution) to the increase in  $\text{CH}_4$  mole fractions at  
 796 Cabauw. The category “rest” primarily represents residential  $\text{CH}_4$  emissions.

797

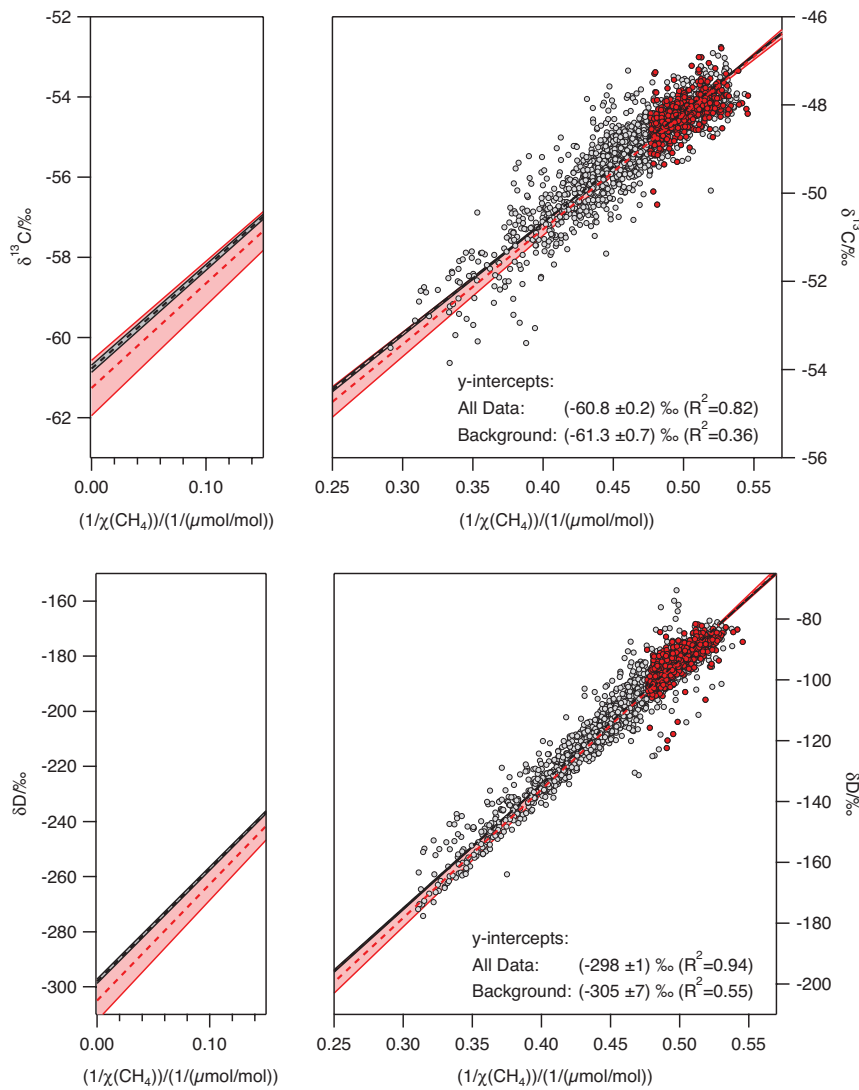


798



799

800 Fig. 5: Comparison of the modeled and measured time series of CH<sub>4</sub> mole fraction  
 801 and isotopic composition ( $\delta^{13}\text{C}$ - and  $\delta\text{D}$ ). Measurements are shown as circles and  
 802 model results as lines. Top graph: two selected model configurations for the  
 803 entire campaign: FLEXPART-COSMO using the TNO-MACC inventory (blue) and  
 804 TM5 using the Edgar/Why-Me inventory (red). Bottom graph: Time series for  
 805 March 2015 with all four model – inventory combinations. For  $\delta\text{D}$ , only the  
 806 synthetic FLEXPART-COSMO results are available for comparison since TM5  
 807 does not simulate  $\delta\text{D}$ .

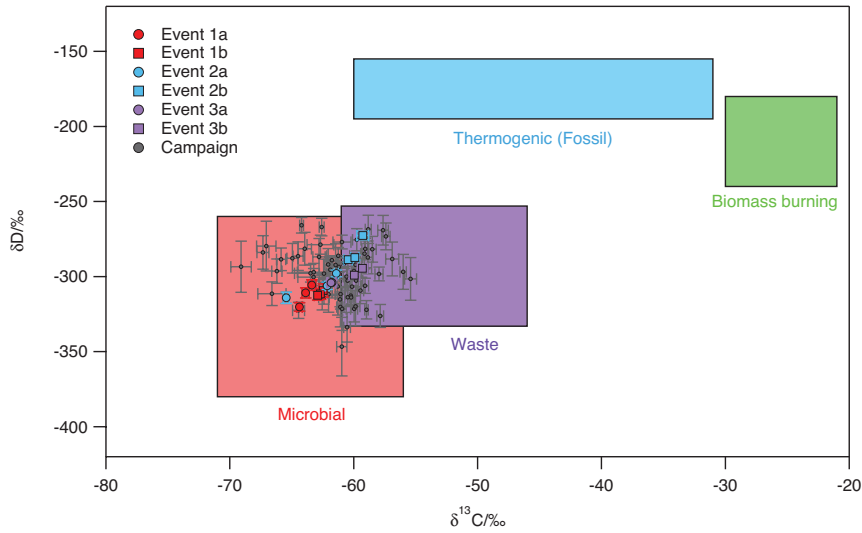


808

809

810 Fig. 6: Keeling plot of all data using an orthogonal regression method. The  
 811 dashed line indicates the regression line and the shaded area the confidence  
 812 interval taking into account the measurement uncertainties. The color code  
 813 indicates all measured data (grey points) and daily background values (red  
 814 points). Left panels show the region near the y-axis intercept.

815



817

818 Fig. 7: MKP intercepts of δD vs. δ¹³C. The colored areas indicate typical isotope  
 819 signatures for different source categories. Circles show the 6h-averaged source  
 820 signatures. Large colored symbols indicate data from the three events (event 1:  
 821 10<sup>th</sup> – 12<sup>th</sup> March, event 2: 16<sup>th</sup> – 18<sup>th</sup> March, event 3: 22<sup>nd</sup> to 24<sup>th</sup> March) that are  
 822 highlighted in Fig. 9. The labels a and b refer to day 1 and day 2 of the two-day  
 823 events, respectively. For the source signatures, the δ¹³C values are taken from  
 824 Table 1 and the δD values from recent literature (Snover et al., 2000; Rigby et al.,  
 825 2012).

826

827

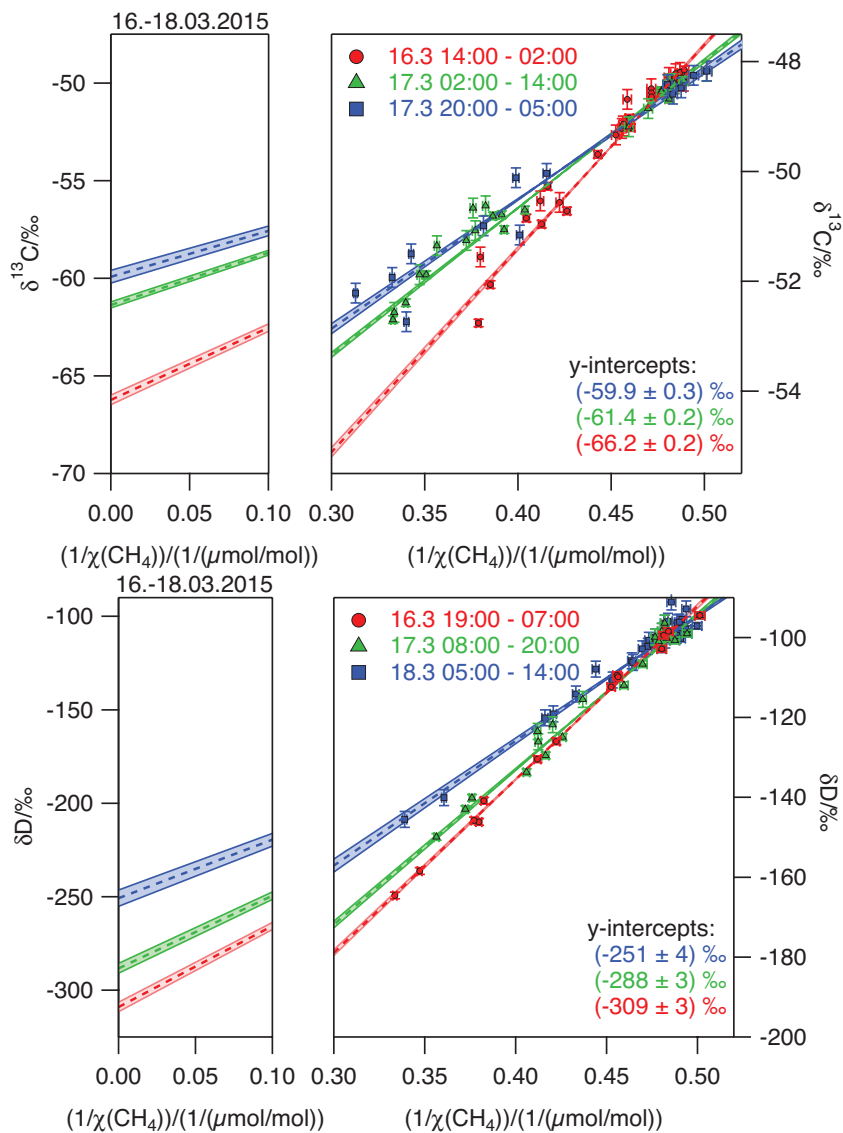
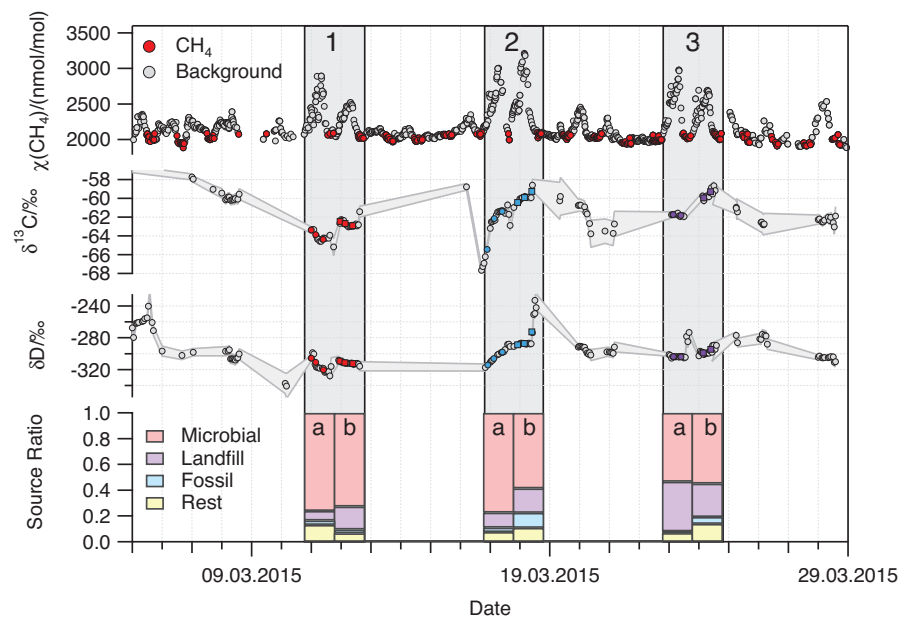


Fig. 8: Keeling plots for the period between 16 and 18 March, illustrating a rapid change in  $\delta$  values over the course of hours, which is most probably related to a change from mainly ruminant derived  $\text{CH}_4$  to a significant contribution of fossil and/or waste  $\text{CH}_4$ . The dashed lines indicate the regression line, the shaded areas show the uncertainty (one standard deviation) of the regression line. Left panels show the region near the y-axis intercept. Times indicated are Central European Time (CET).



838

839

840 Fig. 9: Detailed analysis of three 2-day periods with large CH<sub>4</sub> elevations in  
 841 March 2015. The top panel exhibits CH<sub>4</sub> mole fraction (grey) with background  
 842 values in red (10:00-18:00, >2100 nmol/mol). The middle panels show the mean  
 843 isotopic signatures (δ<sup>13</sup>C, δD) derived with the 12-h MKP method. The color-  
 844 coding in the middle panels (red, light blue, purple) indicates characteristic  
 845 contributions from different sources; red-microbial, light blue-fossil, purple-  
 846 waste. For consistency, the same color-coding was chosen in Fig. 7. The bottom  
 847 graph presents CH<sub>4</sub> source contributions as computed with the FLEXPART-  
 848 COSMO model using the TNO-MACC inventory, averaged over 24 hours.

848

849

850

851

852

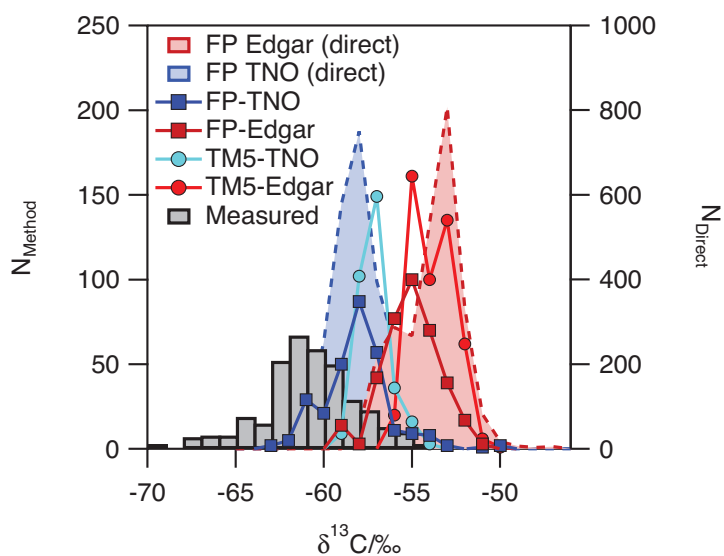
853

854

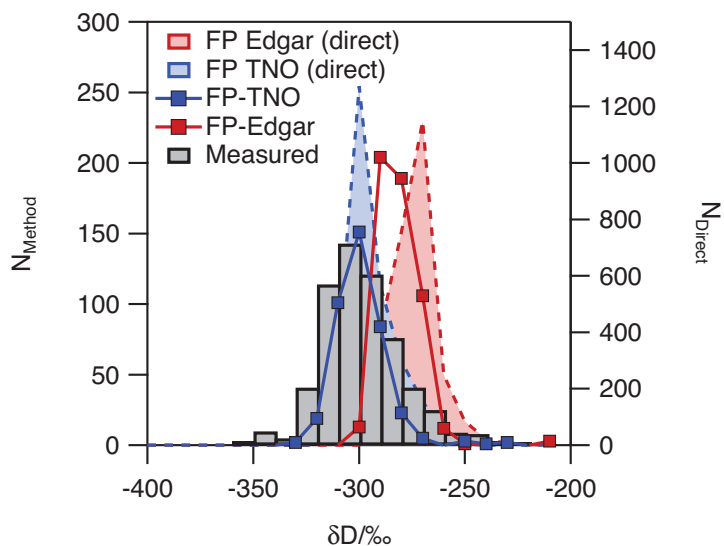
855

856

857



858



859

860 Fig. 10: Histograms of CH<sub>4</sub> isotope source signatures at the CESAR site between  
861 October 2014 and March 2015. Bin widths are 1 ‰ for  $\delta^{13}\text{C}$  and 10 ‰ for  $\delta\text{D}$ .  
862 Mean isotopic signatures are derived from measured data (grey bins),  
863 FLEXPART-COSMO modeling (squares) as well as TM5 modeling (circles) using  
864 the 12 h MKP method. Two different inventories, TNO-MACC (blue) and

865 Edgar/LPJ-Why-Me (red), were used. The shaded areas show histograms for the  
866 “direct” source signatures that were picked up along the FLEXPART-COSMO  
867 trajectory (right axis).

## 868 References

- 869 Baertschi, P.: Absolute  $^{18}\text{O}$  content of Standard Mean Ocean Water, *Earth Planet.*  
870 *Sci. Lett.*, 31, 341-344, 1976.
- 871 Baldauf, M., Seifert, A., Förstner, J., Majewski, D., Raschendorfer, M., and  
872 Reinhardt, T.: Operational Convective-Scale Numerical Weather Prediction with the  
873 COSMO Model: Description and Sensitivities, *Monthly Weather Review*, 139, 3887–  
874 3905, doi:3810.1175/MWR-D-3810-05013.05011, 2011.
- 875 Beck, V., Chen, H. L., Gerbig, C., Bergamaschi, P., Bruhwiler, L., Houweling, S.,  
876 Röckmann, T., Kolle, O., Steinbach, J., Koch, T., Sapart, C. J., van der Veen, C.,  
877 Frankenberg, C., Andreae, M. O., Artaxo, P., Longo, K. M., and Wofsy, S. C.:  
878 Methane airborne measurements and comparison to global models during BARCA, *J.*  
879 *Geophys. Res.*, 117, D15310, doi:15310.11029/12011JD017345, 2012.
- 880 Bergamaschi, P., Brenninkmeijer, C. A. M., Hahn, M., Röckmann, T., Scharffe,  
881 D. H., Crutzen, P. J., Elansky, N. F., Belikov, I. B., Trivett, N. B. A., and Worthy, D.  
882 E. J.: Isotope analysis based source identification for atmospheric  $\text{CH}_4$  and  $\text{CO}$  across  
883 Russia using the Trans-Siberian railroad, *J. Geophys. Res.*, 103, D7, 8227-8235, DOI:  
884 8210.1029/8297JD03738, 1998a.
- 885 Bergamaschi, P., Houweling, S., Segers, A., Krol, M., Frankenberg, C.,  
886 Scheepmaker, R. A., Dlugokencky, E., Wofsy, S. C., Kort, E. A., Sweeney, C.,  
887 Schuck, T., Brenninkmeijer, C., Chen, H., Beck, V., and Gerbig, C.: Atmospheric  
888  $\text{CH}_4$  in the first decade of the 21st century: Inverse modeling analysis using  
889 SCIAMACHY satellite retrievals and NOAA surface measurements, *J Geophys Res-*  
890 *Atmos*, 118, 7350–7369, doi:7310.1002/jgrd.50480, 2013.
- 891 Bergamaschi, P., Lubina, C., Königstedt, R., Fischer, H., Veltkamp, A. C., and  
892 Zwaagstra, O.: Stable isotopic signatures ( $\delta^{13}\text{C}$ ,  $\delta\text{D}$ ) of methane from European  
893 landfill sites, *J. Geophys. Res.*, 103, 8251-8265, doi 8210.1029/8298jd00105, 1998b.
- 894 Bergamaschi, P., Schupp, M., and Harris, G. W.: High-precision direct  
895 measurements of  $^{13}\text{CH}_4/^{12}\text{CH}_4$  and  $\text{CH}_3\text{D}/^{12}\text{CH}_4$  ratios in atmospheric methane  
896 sources by means of a long-path tunable diode laser absorption spectrometer, *Appl.*  
897 *Opt.*, 33, No.33, 7704-7716, 1994.
- 898 Bock, M., Schmitt, J., Behrens, M., Moller, L., Schneider, R., Sapart, C., and  
899 Fischer, H.: A gas chromatography/pyrolysis/isotope ratio mass spectrometry system  
900 for high-precision  $\delta\text{D}$  measurements of atmospheric methane extracted from ice cores,  
901 *Rap. Commun. Mass Spectrom.*, 24, 621-633, 2010.
- 902 Brand, W. A., Rothe, M., Sperlich, P., Strube, M., and Wendeberg, M.:  
903 Automated simultaneous measurement of the  $\delta^{13}\text{C}$  and  $\delta^2\text{H}$  values of methane and the  
904  $\delta^{13}\text{C}$  and  $\delta^{18}\text{O}$  values of carbon dioxide in flask air samples using a new multi cryo-  
905 trap/gas chromatography/isotope ratio mass spectrometry system, *Rapid Commun.*  
906 *Mass Spectrom.*, 30, 1523-1539, doi: 1510.1002/rcm.7587, 2016.
- 907 Brass, M. and Röckmann, T.: Continuous-flow isotope ratio mass spectrometry  
908 method for carbon and hydrogen isotope measurements on atmospheric methane,  
909 *Atmos. Meas. Tech.*, 3, 1707-1721, 2010.



910 Brennkmeijer, C. A. M., Lowe, D. C., Manning, M. R., Sparks, R. J., and  
911 Velthoven, P. F. J. v.: The  $^{13}\text{C}$ ,  $^{14}\text{C}$ , and  $^{18}\text{O}$  isotopic composition of  $\text{CO}$ ,  $\text{CH}_4$  and  
912  $\text{CO}_2$  in the higher southern latitudes lower stratosphere, *J. Geophys. Res.*, 100,  
913 26,163-126,172, 1995.

914 Bruhwiler, L., Dlugokencky, E., Masarie, K., Ishizawa, M., Andrews, A., Miller,  
915 J., Sweeney, C., Tans, P., and Worthy, D.: CarbonTracker- $\text{CH}_4$ : an assimilation  
916 system for estimating emissions of atmospheric methane, *Atmos. Chem. Phys.*, 14,  
917 8269-8293, 2014.

918 Craig, H.: Isotopic standards for carbon and oxygen and correction factors for  
919 mass-spectrometric analysis of carbon dioxide, *Geochim. Cosmochim. Acta*, 12, 133-  
920 149, 1957.

921 Dee, D. P., Uppala, S. M., Simmons, A. J., Berrisford, P., Poli, P., and al., e.: The  
922 ERA-Interim reanalysis: configuration and performance of the data assimilation  
923 system, *Quart. J. Roy. Meteor. Soc.*, 553-579, 2011.

924 Dlugokencky, E. J., Bruhwiler, L., White, J. W. C., Emmons, L. K., Novelli, P.  
925 C., Montzka, S. A., Masarie, K. A., Lang, P. M., Crotwell, A. M., Miller, J. B., and  
926 Gatti, L. V.: Observational constraints on recent increases in the atmospheric  $\text{CH}_4$   
927 burden, *Geophys. Res. Lett.*, 36, L18803, doi 18810.11029/12009gl039780, 2009.

928 Dlugokencky, E. J., Dutton, E. G., Novelli, P. C., Tans, P. P., Masarie, K. A.,  
929 Lantz, K. O., and Madronich, S.: Changes in  $\text{CH}_4$  and  $\text{CO}$  growth rates after the  
930 eruption of Mt. Pinatubo and their link with changes in tropical tropospheric UV flux,  
931 *Geophys. Res. Lett.*, 23, 2761-2764, 1996.

932 Dlugokencky, E. J., Masarie, K. A., Lang, P. M., and Tans, P. P.: Continuing  
933 decline in the growth rate of the atmospheric methane burden, *Nature*, 393, 447-450,  
934 1998.

935 Dlugokencky, E. J., Myers, R. C., Lang, P. M., Masarie, K. A., Crotwell, A. M.,  
936 Thoning, K. W., Hall, B. D., Elkins, J. W., and Steele, L. P.: Conversion of NOAA  
937 atmospheric dry air  $\text{CH}_4$  mole fractions to a gravimetrically prepared standard scale, *J.*  
938 *Geophys. Res.*, 110, D18306, Doi 18310.11029/12005jd006035, 2005.

939 EDGAR: European Commission, Joint Research Centre (JRC)/Netherlands  
940 Environmental Assessment Agency (PBL). , Emission Database for Global  
941 Atmospheric Research (EDGAR), Version 4.2. , 2010. Available at  
942 <http://edgar.jrc.ec.europa.eu>, 2010.

943 EDGAR: European Commission, Joint Research Centre (JRC)/Netherlands  
944 Environmental Assessment Agency (PBL). Emission Database for Global  
945 Atmospheric Research (EDGAR), release version 4.2.  
946 <http://edgar.jrc.ec.europa.eu>, 2009.

947 Etheridge, D. M., Steele, L. P., Francey, R. J., and Langenfelds, R. L.:  
948 Atmospheric methane between 1000 AD and present: Evidence of antropogenic  
949 emissions and climatic variability, *J. Geophys. Res.*, 103, 15979-15993, 1998.

950 Etiope, G., Lassey, K. R., Klusman, R. W., and Boschi, E.: Reappraisal of the  
951 fossil methane budget and related emission from geologic sources, *Geophys. Res.*  
952 *Lett.*, 35, 2008.

953 Eyer, S. and al, e.: Real-time analysis of  $\delta^{13}\text{C}$ - and  $\delta\text{D-CH}_4$  in ambient air with  
954 laser spectroscopy: Method development and first intercomparison results., *Atmos.*  
955 *Meas. Tech. Discuss.*, 8, 8925-8970, 2015.

956 Eyer, S., Stadie, N. P., Borgschulte, A., Emmenegger, L., and Mohn, J.: Methane  
957 pre-concentration by adsorption: a methodology for materials and conditions selection,  
958 *Adsorption-Journal of the International Adsorption Society*, 20, 657-666, 2014.

959 Ferretti, D., Miller, J., White, J., Etheridge, D., Lassey, K., Lowe, D., Allan, B.,  
960 MacFarling, C., Dreier, M., Trudinger, C., and Ommen, T. v.: Unexpected changes to  
961 the global methane budget over the past 2000 years, *Science*, 309, 1714-1717, 2005.

962 Fischer, H., Behrens, M., Bock, M., Richter, U., Schmitt, J., Louergue, L.,  
963 Chappellaz, J., Spahni, R., Blunier, T., Leuenberger, M., and Stocker, T. F.: Changing  
964 boreal methane sources and constant biomass burning during the last termination,  
965 *Nature*, 452, 864-867, 2008.

966 Gros, V., Brenninkmeijer, C. A. M., Jöckel, P., Kaiser, J., Lowry, D., Nisbet, E.  
967 G., O'Brian, P., Röckmann, T., and Warwick, N.: Isotope signatures of trace gas  
968 sources. In: *Emissions Of Atmospheric Trace Compounds*, Granier, C., Artaxo, P.,  
969 and Reeves, C. E. (Eds.), *Advances in Global Change Research*, Kluwer Academic  
970 Pub., Paris, 2004.

971 Henne, S., Brunner, D., Oney, B., Leuenberger, M., Eugster, W., Bamberger, I.,  
972 Meinhardt, F., Steinbacher, M., and Emmenegger, L.: Validation of the Swiss  
973 methane emission inventory by atmospheric observations and inverse modelling,  
974 *Atmos. Chem. Phys. Discuss.*, 2015. 35417-35484, doi:35410.35194/acpd-35415-  
975 35417-32015, 2015.

976 Hiller, R. V., Bretscher, D., DelSontro, T., Diem, T., Eugster, W., Henneberger,  
977 R., Hobi, S., Hodson, E., Imer, D., Kreuzer, M., Künzle, T., Merbold, L., Niklaus, P.  
978 A., Rihm, B., Schellenberger, A., Schroth, M. H., Schubert, C. J., Siegrist, H., Stieger,  
979 J., Buchmann, N., and Brunner, D.: Anthropogenic and natural methane fluxes in  
980 Switzerland synthesized within a spatially explicit inventory, *Biogeosciences*, 11,  
981 1941-1959, doi:1910.5194/bg-1911-1941-2014, 2014.

982 Houweling, S., Krol, M., Bergamaschi, P., Frankenberg, C., Dlugokencky, E. J.,  
983 Morino, I., Notholt, J., Sherlock, V., Wunch, D., Beck, V., Gerbig, C., Chen, H., Kort,  
984 E. A., Röckmann, T., and Aben, I.: A multi-year methane inversion using  
985 SCIAMACHY, accounting for systematic errors using TCCON measurements,  
986 *Atmos. Chem. Phys.*, 14, 3991-4012, 2014.

987 Houweling, S., van der Werf, G. R., Goldewijk, K. K., Röckmann, T., and Aben,  
988 I.: Early anthropogenic CH<sub>4</sub> emissions and the variation of CH<sub>4</sub> and <sup>13</sup>CH<sub>4</sub> over the  
989 last millennium, *Global Biogeochem Cy*, 22, 2008.

990 Kawagucci, S., Kobayashi, M., Hattori, S., Yamada, K., Ueno, Y., Takai, K., and  
991 Yoshida, N.: Hydrogen isotope systematics among H<sub>2</sub>-H<sub>2</sub>O-CH<sub>4</sub> during the growth of  
992 the hydrogenotrophic methanogen *Methanothermobacter thermoautotrophicus* strain  
993 Delta H, *Geochim Cosmochim Acta*, 142, 601-614, 2014.

994 Keeling, C. D.: The Concentration and Isotopic Abundances of Carbon Dioxide  
995 in Rural and Marine Air, *Geochim. Cosmochim. Acta*, 24, 277-298, 1961.

996 Khalil, M. A. K., Butenhoff, C. L., and Rasmussen, R. A.: Atmospheric methane:  
997 Trends and cycles of sources and sinks, *Environmental Science & Technology*, 41,  
998 2131-2137, 2007.

999 Kirschke, S., Bousquet, P., Ciais, P., Saunoy, M., Canadell, J. G., Dlugokencky,  
1000 E. J., Bergamaschi, P., Bergmann, D., Blake, D. R., Bruhwiler, L., Cameron-Smith,  
1001 P., Castaldi, S., Chevallier, F., Feng, L., Fraser, A., Heimann, M., Hodson, E. L.,  
1002 Houweling, S., Josse, B., Fraser, P. J., Krummel, P. B., Lamarque, J. F., Langenfelds,  
1003 R. L., Le Quere, C., Naik, V., O'Doherty, S., Palmer, P. I., Pison, I., Plummer, D.,

1004 Poulter, B., Prinn, R. G., Rigby, M., Ringeval, B., Santini, M., Schmidt, M., Shindell,  
1005 D. T., Simpson, I. J., Spahni, R., Steele, L. P., Strode, S. A., Sudo, K., Szopa, S., van  
1006 der Werf, G. R., Voulgarakis, A., van Weele, M., Weiss, R. F., Williams, J. E., and  
1007 Zeng, G.: Three decades of global methane sources and sinks, *Nat Geosci*, 6, 813-823,  
1008 2013.

1009 Klevenhusen, F., Bernasconi, S. M., Kreuzer, M., and Soliva, C. R.: Experimental  
1010 validation of the Intergovernmental Panel on Climate Change default values for  
1011 ruminant-derived methane and its carbon-isotope signature, *Anim Prod Sci*, 50, 159-  
1012 167, 2010.

1013 Krol, M., Houweling, S., Bregman, B., van den Broek, M., Segers, A., van  
1014 Velthoven, P., Peters, W., Dentener, F., and Bergamaschi, P.: The two-way nested  
1015 global chemistry-transport zoom model TM5: algorithm and applications, *Atmos.*  
1016 *Chem. Phys.*, 5, 417-432, 2005.

1017 Kuenen, J. J. P., Visschedijk, A. J. H., Jozwicka, M., and van der Gon, H. A. C.  
1018 D.: TNO-MACC\_II emission inventory; a multi-year (2003-2009) consistent high-  
1019 resolution European emission inventory for air quality modelling, *Atmos. Chem.*  
1020 *Phys.*, 14, 10963-10976, 2014.

1021 Lassey, K. R., Lowe, D. C., Brenninkmeijer, C. A. M., and Gomez, A. J.:  
1022 Atmospheric Methane and its Carbon Isotopes in the Southern Hemisphere: their  
1023 Time Series and an Instructive Model, *Chemosphere*, 26, 95-109, 1993.

1024 Lassey, K. R., Lowe, D. C., and Manning, M. R.: The trend in atmospheric  
1025 methane  $\delta^{13}\text{C}$  implications for isotopic constraints on the global methane budget,  
1026 *Global Biogeochem Cy*, 14, 41-49, 2000.

1027 Loulergue, L., Schilt, A., Spahni, R., Masson-Delmotte, V., Blunier, T., Lemieux,  
1028 B., Barnola, J. M., Raynaud, D., Stocker, T. F., and Chappellaz, J.: Orbital and  
1029 millennial-scale features of atmospheric  $\text{CH}_4$  over the past 800,000 years, *Nature*,  
1030 453, 383-386, 2008.

1031 Lowe, D. C., Brenninkmeijer, C. A. M., Brailsford, G. W., Lassey, K. R., Gomez,  
1032 A. J., and Nisbet, E. G.: Concentration and  $^{13}\text{C}$  Records of Atmospheric Methane in  
1033 New-Zealand and Antarctica - Evidence for Changes in Methane Sources, *J. Geophys.*  
1034 *Res.*, 99, 16913-16925, 1994.

1035 MacFarling Meure, C., Etheridge, D., Trudinger, C., Steele, P., Langenfelds, R.,  
1036 Ommen, T. v., Smith, A., and Elkins, J.: Law Dome  $\text{CO}_2$ ,  $\text{CH}_4$  and  $\text{N}_2\text{O}$  ice core  
1037 records extended to 2000 years BP *Geophys. Res. Lett.*, 33, L14810,  
1038 doi:14810.11029/12006GL026152 2006.

1039 Merritt, D. A., Brand, W. A., and Hayes, J. M.: Isotope-ratio-monitoring gas  
1040 chromatography-mass spectrometry: methods for isotopic calibration, *Org. Geochem.*,  
1041 21 No. 6/7, 573-583, 1994.

1042 Merritt, D. A., Hayes, J. M., and Des Marais, D. J.: Carbon isotopic analysis of  
1043 atmospheric methane by isotope-ratio-monitoring gas chromatography-mass  
1044 spectrometry, *J. Geophys. Res.*, 100 D, 1317-1326, 1995.

1045 Mohn, J., Guggenheim, C., Tuzson, B., Vollmer, M. K., Toyoda, S., Yoshida, N.,  
1046 and Emmenegger, L.: A liquid nitrogen-free preconcentration unit for measurements  
1047 of ambient  $\text{N}_2\text{O}$  isotopomers by QCLAS, *Atmos Meas Tech*, 3, 609-618, 2010.

1048 Mohn, J., Tuzson, B., Manninen, A., Yoshida, N., Toyoda, S., Brand, W. A., and  
1049 Emmenegger, L.: Site selective real-time measurements of atmospheric  $\text{N}_2\text{O}$   
1050 isotopomers by laser spectroscopy, *Atmos Meas Tech*, 5, 1601-1609, 2012.

1051 Monteil, G., Houweling, S., Dlugokenky, E. J., Maenhout, G., Vaughn, B. H.,  
1052 White, J. W. C., and Röckmann, T.: Interpreting methane variations in the past two  
1053 decades using measurements of CH<sub>4</sub> mixing ratio and isotopic composition, *Atmos.*  
1054 *Chem. Phys.*, 11, 9141-9153, 2011.

1055 Monteil, G., Houweling, S., Guerlet, S., Schepers, D., Frankenberg, C.,  
1056 Scheepmaker, R., Aben, I., Butz, A., Hasekamp, O., Landgraf, J., Wofsy, S. C., and  
1057 Röckmann, T.: Intercomparison of 15 months inversions of GOSAT and  
1058 SCIAMACHY CH<sub>4</sub> retrievals, *J. Geophys. Res.*, 118, 11807-11823,  
1059 doi:10.1029/2013JD019760, 2013.

1060 Nisbet, E. G., Dlugokenky, E. J., and Bousquet, P.: Methane on the rise—again,  
1061 *Science*, 343, 493-495, 2014.

1062 Pataki, D. E., Ehleringer, J. R., Flanagan, L. B., Yakir, D., Bowling, D. R., Still,  
1063 C. J., Buchmann, N., Kaplan, J. O., and Berry, J. A.: The application and  
1064 interpretation of Keeling plots in terrestrial carbon cycle research, *Global*  
1065 *Biogeochem Cy*, 17, 1022, doi:10.1029/2001GB001850, 2003.

1066 Peltola, O., Hensen, A., Helfter, C., Marchesini, L. B., Bosveld, F. C., van den  
1067 Bulk, W. C. M., Elbers, J. A., Haapanala, S., Holst, J., Laurila, T., Lindroth, A.,  
1068 Nemitz, E., Röckmann, T., Vermeulen, A. T., and Mammarella, I.: Evaluating the  
1069 performance of commonly used gas analysers for methane eddy covariance flux  
1070 measurements: the InGOS inter-comparison field experiment, *Biogeosciences*, 11,  
1071 3163-3186, 2014.

1072 Peltola, O., Hensen, A., Marchesini, L. B., Helfter, C., Bosveld, F. C., van den  
1073 Bulk, W. C. M., Haapanala, S., van Huissteden, J., Laurila, T., Lindroth, A., Nemitz,  
1074 E., Röckmann, T., Vermeulen, A. T., and Mammarella, I.: Studying the spatial  
1075 variability of methane flux with five eddy covariance towers of varying height,  
1076 *Agricultural and Forest Meteorology*, 214, 456-472, 2015.

1077 Quay, P., Stutsman, J., Wilbur, D., Snover, A., Dlugokenky, E., and Brown, T.:  
1078 The isotopic composition of atmospheric methane, *Global Biogeochem Cy*, 13, 445-  
1079 461, 1999.

1080 Rasmussen, R. A. and Khalil, M. A. K.: Atmospheric Methane (CH<sub>4</sub>) - Trends  
1081 and Seasonal Cycles, *J. Geophys. Res.*, 86, 9826-9832, 1981.

1082 Rigby, M., Manning, A. J., and Prinn, R. G.: The value of high-frequency, high-  
1083 precision methane isotopologue measurements for source and sink estimation, *J.*  
1084 *Geophys. Res.*, 117, 2012.

1085 Röckmann, T., Brass, M., Borchers, R., and Engel, A.: The isotopic composition  
1086 of methane in the stratosphere: High-altitude balloon sample measurements, *Atm.*  
1087 *Chem. Phys.*, 11, 13287-13304, 2011.

1088 Sanderson, M. G.: Biomass of termites and their emissions of methane and  
1089 carbon dioxide: A global database, *Global Biogeochem. Cycles*, 10, 543-557, 1996.

1090 Sapart, C. J., Monteil, G., Prokopiou, M., van de Wal, R. S. W., Kaplan, J. O.,  
1091 Sperlich, P., Krumhardt, K. M., van der Veen, C., Houweling, S., Krol, M. C.,  
1092 Blunier, T., Sowers, T., Martinerie, P., Witrant, E., Dahl-Jensen, D., and Röckmann,  
1093 T.: Natural and anthropogenic variations in methane sources during the past two  
1094 millennia, *Nature*, 490, 85-88, 2012.

1095 Sapart, C. J., Veen, C. v. d., Vigano, I., Brass, M., Wal, R. S. W. v. d., Bock, M.,  
1096 Fischer, H., Sowers, T., Buizert, C., Sperlich, P., Blunier, T., Behrens, M., Schmitt, J.,

1097 Seth, B., and Röckmann, T.: Simultaneous stable isotope analysis of methane and  
1098 nitrous oxide on ice core samples, *Atmos. Meas. Tech.*, 4, 2607-2618, 2011.

1099 Saueressig, G., Bergamaschi, P., Crowley, J. N., Fischer, H., and Harris, G. W.:  
1100 D/H kinetic isotope effect in the reaction  $\text{CH}_4 + \text{Cl}$ , *Geophys. Res. Lett.*, 23, 3619-  
1101 3622, 1996.

1102 Saueressig, G., Crowley, J. N., Bergamaschi, P., Brühl, C., Brenninkmeijer, C. A.  
1103 | M., and Fischer, H.: Carbon 13 and D kinetic isotope effects in the reactions of  $\text{CH}_4$   
1104 with  $\text{O}(^1\text{D})$  and OH: New laboratory measurements and their implications for the  
1105 isotopic composition of stratospheric methane, *J. Geophys. Res.*, 106, 23127-23138,  
1106 2001.

1107 Schmitt, J., Seth, B., Bock, M., van der Veen, C., Möller, L., Sapart, C. J.,  
1108 Prokopiou, M., Sowers, T., Röckmann, T., and Fischer, H.: On the interference of Kr  
1109 during carbon isotope analysis of methane using continuous-flow combustion-isotope  
1110 ratio mass spectrometry, *Atmos. Meas. Tech.*, 6, 1425-1445, 2013.

1111 Seibert, P. and Frank, A.: Source-receptor matrix calculation with a Lagrangian  
1112 particle dispersion model in backward mode, *Atmos. Chem. Phys.*, 4, 51-63, 2004.

1113 Snover, A. K. and Quay, P. D.: Hydrogen and carbon kinetic isotope effects  
1114 during soil uptake of atmospheric methane, *Global Biogeochem. Cycles*, 14, 25-39,  
1115 2000.

1116 Spahni, R., Chappellaz, J., Stocker, T. F., Louergue, L., Hausammann, G.,  
1117 Kawamura, K., Flückiger, J., Schwander, J., Raynaud, D., Masson-Delmotte, V., and  
1118 Jouzel, J.: Atmospheric Methane and Nitrous Oxide of the Late Pleistocene from  
1119 Antarctic Ice Cores, *Science*, 310, 1317-1321, DOI: 1310.1126/science.1120132,  
1120 2005.

1121 Spahni, R., Wania, R., Neef, L., Weele, M. v., Pison, I., Bousquet, P.,  
1122 Frankenberg, C., Foster, P. N., Joos, F., Prentice, I. C., and Velthoven, P. v.:  
1123 Constraining global methane emissions and uptake by ecosystems, *Biogeosciences*, 8,  
1124 1643-1665, doi:1610.5194/bg-1648-1643-2011., 2011.

1125 Sperlich, P., Buizert, C., Jenk, T. M., Sapart, C. J., Prokopiou, M., Röckmann, T.,  
1126 and Blunier, T.: An automated GC-C-GC-IRMS setup to measure palaeoatmospheric  
1127  $\delta^{13}\text{C}-\text{CH}_4$ ,  $\delta^{15}\text{N}-\text{N}_2\text{O}$  and  $\delta^{18}\text{O}-\text{N}_2\text{O}$  in one ice core sample, *Atmos Meas Tech*, 6,  
1128 2027-2041, 2013.

1129 Sperlich, P., Uitslag, N. A. M., Richter, J. M., Rothe, M., Geilmann, H., Veen, C.  
1130 v., Röckmann, T., Blunier, T., and Brand, W. A.: Development and evaluation of a  
1131 suite of isotope reference gases for methane in air, submitted to *Atmos. Meas. Tech.*  
1132 *Disc.*, 2016. 2016.

1133 Stohl, A., Forster, C., Frank, A., Seibert, P., and Wotawa, G.: Technical note: The  
1134 Lagrangian particle dispersion model FLEXPART version 6.2, *Atmos. Chem. Phys.*,  
1135 5, 2461-2474, 2005.

1136 Sturm, P., Tuzson, B., Henne, S., and Emmenegger, L.: Tracking isotopic  
1137 signatures of  $\text{CO}_2$  at the high altitude site Jungfraujoch with laser spectroscopy:  
1138 analytical improvements and representative results, *Atmos. Meas. Tech.*, 6, 1659-  
1139 1671, 2013.

1140 Tarasova, O. A., Brenninkmeijer, C. A. M., Assonov, S. S., Elansky, N. F.,  
1141 Röckmann, T., and Brass, M.: Atmospheric  $\text{CH}_4$  along the Trans-Siberian railroad  
1142 (TROICA) and river Ob: Source identification using stable isotope analysis, *Atmos.*  
1143 *Environ.*, 40, 5617-5628, 2006.

1144 Tuzson, B., Henne, S., Brunner, D., Steinbacher, M., Mohn, J., Buchmann, B.,  
1145 and Emmenegger, L.: Continuous isotopic composition measurements of tropospheric  
1146 CO<sub>2</sub> at Jungfraujoch (3580 m a.s.l.), Switzerland: real-time observation of regional  
1147 pollution events, *Atmos. Chem. Phys.*, 11, 1685-1696, 2011.

1148 Tuzson, B., Mohn, J., Zeeman, M. J., Werner, R. A., Eugster, W., Zahniser, M.  
1149 S., Nelson, D. D., McManus, J. B., and Emmenegger, L.: High precision and  
1150 continuous field measurements of  $\delta^{13}\text{C}$  and  $\delta^{18}\text{O}$  in carbon dioxide with a cryogen-  
1151 free QCLAS, *Appl. Phys. B-Lasers and Optics*, 92, 451-458, 2008.

1152 Umezawa, T., Aoki, S., Nakazawa, T., and Morimoto, S.: A High-precision  
1153 Measurement System for Carbon and Hydrogen Isotopic Ratios of Atmospheric  
1154 Methane and Its Application to Air Samples Collected in the Western Pacific Region,  
1155 *Journal of the Meteorological Society of Japan*, 87, 365-379, 2009.

1156 Umezawa, T., Machida, T., Aoki, S., and Nakazawa, T.: Contributions of natural  
1157 and anthropogenic sources to atmospheric methane variations over western Siberia  
1158 estimated from its carbon and hydrogen isotopes, *Global Biogeochem. Cycles*, 26,  
1159 2012a.

1160 Umezawa, T., Machida, T., Ishijima, K., Matsueda, H., Sawa, Y., Patra, P. K.,  
1161 Aoki, S., and Nakazawa, T.: Carbon and hydrogen isotopic ratios of atmospheric  
1162 methane in the upper troposphere over the Western Pacific, *Atmos. Chem. Phys.*, 12,  
1163 8095-8113, 2012b.

1164 Vermeulen, A. T., Hensen, A., Popa, M. E., van den Bulk, W. C. M., and  
1165 Jongejan, P. A. C.: Greenhouse gas observations from Cabauw Tall Tower (1992-  
1166 2010), *Atmos. Meas. Tech.*, 4, 617-644, 2011.

1167 Wächter, H., Mohn, J., Tuzson, B., Emmenegger, L., and Sigrist, M. W.:  
1168 Determination of N<sub>2</sub>O isotopomers with quantum cascade laser based absorption  
1169 spectroscopy, *Optics Express*, 16, 9239-9244, 2008.

1170 WMO: 17th WMO/IAEA Meeting on Carbon Dioxide, Other Greenhouse Gases,  
1171 and Related Measurement Techniques (GGMT-2013) 10-13 June 2013, GAW Report  
1172 No. 213., World Meteorological Organization, Geneva, Switzerland, Beijing, China,  
1173 2014.

1174 Wolf, B., Merbold, L., Decock, C., Tuzson, B., Harris, E., Six, J., Emmenegger,  
1175 L., and Mohn, J.: First on-line isotopic characterization of N<sub>2</sub>O above intensively  
1176 managed grassland, *Biogeosciences*, 12, 2517-2531, 2015.

1177 Yamada, K., Ozaki, Y., Nakagawa, F., Tanaka, M., and Yoshida, N.: An  
1178 improved method for measurement of the hydrogen isotope ratio of atmospheric  
1179 methane and its application to a Japanese urban atmosphere, *Atmos. Environ.*, 37,  
1180 1975-1982, 2003.

1181 Zazzeri, G., Lowry, D., Fisher, R. E., France, J. L., Lanoiselle, M., and Nisbet, E.  
1182 G.: Plume mapping and isotopic characterisation of anthropogenic methane sources,  
1183 *Atmos. Environ.*, 110, 151-162, 2015.

1184